The evolution of late-Hercynian granites and rhyolites documented by quartz – a review

Axel Müller[1], Alfons M. van den Kerkhof[2], Hans-Jürgen Behr[2], Andreas Kronz[2], Monika Koch-Müller[3]

[1] Geological Survey of Norway, N-7491 Trondheim, Norway
[2] Geowissenschaftliches Zentrum Göttingen, Goldschmidtstr. 3, D-37073 Göttingen, Germany
[3] GeoForschungsZentrum Potsdam, Telegrafenberg, D-14473 Potsdam, Germany

ABSTRACT: The potential of igneous quartz for providing a better understanding of magmatic processes is demonstrated by studying late-Hercynian rhyolites and granites from central and western Europe. Cathodoluminescence (CL) reveals growth patterns and alteration structures within igneous quartz reflecting the magma crystallisation history. The relatively stable and blue-dominant CL of zoned phenocrysts is principally related to variations in the Ti concentration, which is a function of the crystallisation temperature. The Al/Ti ratio of igneous quartz increases with progressive magma differentiation, as Ti is more compatible, compared to Al, Li, K, Ge, B, Fe, P during magma evolution. The red-dominant CL of the anhedral groundmass quartz in granite is unstable during electron bombardment and associated with OH- and H_2O-bearing lattice defects. Thus, CL properties of quartz are different for rocks formed from H_2O-poor and H_2O-rich melts. Both groundmass and phenocrysts in granites are rich in alteration structures as a result of interaction with deuteric fluids during cooling, whereas phenocrysts in extrusive rocks do not usually contain such structures. The combined study of trace elements along with the analysis of quartz textures and melt inclusion inventories may reveal detailed PTX-paths of granite magmas. This study shows that quartz is a sensitive indicator for physico-chemical changes during the evolution of silica-rich magmas. Common growth textures show a wide variety in quartz phenocrysts in rhyolites and some granites. We present a classification of textures, which formed as a result of heterogeneous intra-granular lattice defects and impurities. The alternation of growth and resorption microtextures reflects stepwise adiabatic and non-adiabatic magma ascent, temporary storage of magma in reservoirs and mixing with more mafic, hotter magma. The anhedral groundmass quartz overgrowing early-magmatic phenocrysts in granites is free of growth zoning.

KEY WORDS: adiabatic, cathodoluminescence, crystal resorption, growth textures, late-Hercynian magmatism, quartz

1. Introduction

Quartz provides a detailed chronicle of physicochemical changes in granitic melts. Quartz phenocrysts normally grow in different magma batches, which are repeatedly recharged. The solidified granites and rhyolites therefore comprise mixtures of different phenocryst populations embedded in a microcrystalline to coarse-grained groundmass. Feldspars in granites and rhyolites are commonly altered due to the late- to post-magmatic interaction with deuteric and hydrothermal fluids. Quartz is more resistant in this environment with the consequence that magmatic zoning patterns are commonly preserved. These patterns can be revealed by cathodoluminescence (CL) techniques.

Information about the physicochemical changes during the evolution of granitic magma can be obtained by the study of (1) growth patterns in quartz as visualised by cathodoluminescence, (2) trace element concentrations and distribution within quartz crystals, and (3) melt inclusions hosted by quartz.

(1) Laemmlein (1930) examined by optical microscope - probably for the first time - primary growth structures in quartz phenocrysts in rhyolite from Transbaikalia. It was until the 1980/90s, however, that growth zoning (Schneider 1993; D'Lemos *et al.* 1997; Watt *et al.* 1997) and alteration textures (Sprunt & Nur 1979; Behr 1989; Behr & Frentzel-Beyme 1989) in igneous quartz were studied in more detail by CL microscopy. During the last decade CL microscopy has become a routine method to visualise growth and alteration patterns in igneous quartz (Müller *et al.* 2000, 2002a, 2003b, 2005; Peppard *et al.* 2001; Ruffini *et al.* 2002; Wark *et al.* 2007; Wiebe *et al.* 2007). CL reveals episodes of quartz crystallisation including crystal nucleation, growth and dissolution, which develop during magma ascent, storage, recharge, and mixing. The effects of late- to post-magmatic quartz alteration become also visible in CL studies.

(2) CL colour and intensity are the result of intrinsic lattice defects (*e.g.,* oxygen and silicon vacancies, broken bonds) as well as trace elements in the crystal structure (*e.g*., Sprunt 1981; Ramseyer *et al.* 1988; Perny *et al.* 1992; Stevens Kalceff *et al.* 2000; Götze *et al.* 2001, 2004, 2005). However, the physical background of quartz luminescence has not been fully understood. The concentration of trace elements in quartz is controlled by their abundance in the melt, the partitioning between different phases, and the thermodynamic conditions in the system (Müller *et al.* 2000, 2002a, 2003b; Jacamon & Larsen 2009; Wark *et al.* 2007). Several attempts have been made to combine CL and trace element analysis allowing the quantitative measurement of the Al, Ti, K, and Fe distribution of quartz in relation to CL textures (Watt *et al.* 1997; Müller *et al.* 2000, 2002a, 2003b; Ruffini *et al.* 2002; Wark *et al.* 2007; Wiebe *et al.* 2007). In other studies the total content of Al, Ti, Ge, and Li of igneous quartz has been used to discriminate among magmas of different origin, or in order to better understand the fractionation process (Lyakhovich 1972; Suttner & Leininger 1972; Schrön *et al.* 1988; Gurbanov *et al.* 1999; Larsen *et al.* 2000, 2004; Götze *et al.* 2004; Jacamon & Larsen 2009). Wark & Watson (2006) established the Ti-in-quartz geothermometer, which allows the calculation of the magma temperature at different stages of quartz growth. The incorporation of Al into the quartz lattice is probably controlled by the aluminium saturation index of the magma (Jacamon & Larsen 2009).

(3) Igneous quartz, in particular phenocrystic quartz, contains melt inclusions. Melt inclusions comprise a unique record of melt and volatile contents prior to magma emplacement. They record the evolving melt composition and can be used for magma pressure estimates in relation to quartz growth zones. In their study on the Bishop tuff (eastern California, USA) Peppard *et al.* (2001) related different melt inclusions to growth zones in quartz phenocrysts.

Wark *et al.* (2007) continued their work and applied the Ti-in-quartz thermometer to explain variations of the volatile content in melt inclusions. They showed that quartz phenocryst rims containing CO_2-rich melt inclusions document an ~100°C increase of magma temperature shortly prior to eruption.
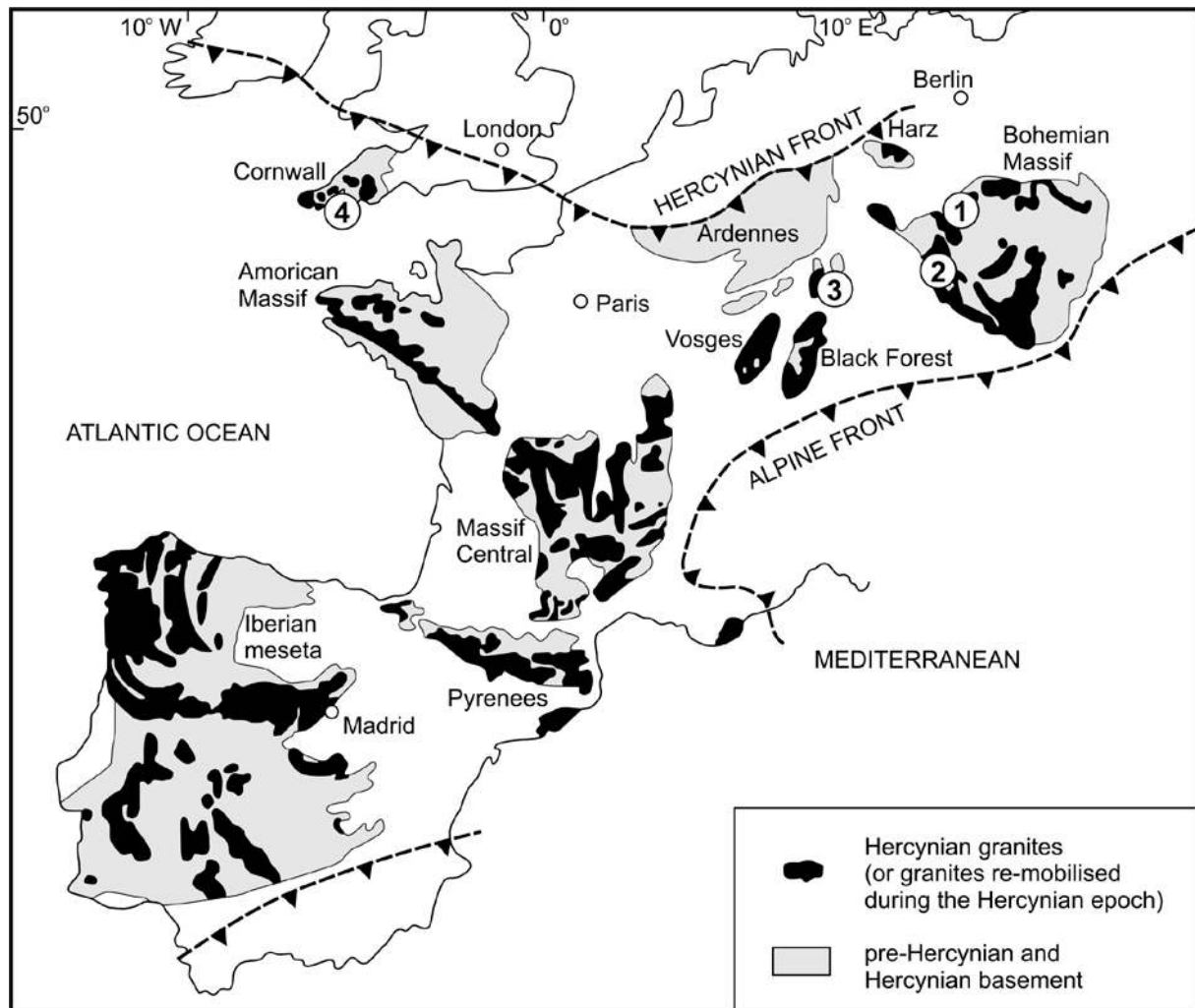

Figure 1 The Hercynian Europe according Rajpoot (1991) with sample locations: 1 – Erzgebirge/Krušné Hory, 2 - Oberpfalz, 3 – Odenwald, and 4 - Cornwall.

The aim of the present study is to reveal the magmatogenetic significance of CL properties and textures in relation to the trace element distribution of igneous quartz in late-Hercynian (Upper Carboniferous to Lower Permian) felsic plutonic and volcanic rocks. Furthermore, the paper compiles the results of a number of earlier studies on growth structures and the microchemistry of igneous quartz (Müller 2000; Müller *et al.* 2000, 2002a, 2003b, 2005, 2006a). Samples are collected from the Erzgebirge, Oberpfalz, and Odenwald (Germany), and from Cornwall (SW England, Fig. 1). As a reference some intermediate to felsic plutonic rocks and associated volcanic rocks of different age and tectonic settings have been included. These rocks (1) are well studied in respect to age, chemical evolution and tectonic setting, (2) cover a wide range of chemical variability from dioritic/dacitic to highly evolved granitic/rhyolitic compositions, (3) include both plutonic and associated volcanic rocks, (4) show well-developed quartz textures (Müller *et al.* 2000, 2002a, 2003b, 2005), and (5) have melt inclusion data available (Thomas 1992, 1994; Müller *et al.* 2006b).

In this study we combined several visualising and micro-analytical methods, i.e. scanning electron microscope cathodoluminescence (SEM-CL) and optical microscope CL (OM-CL) combined with Fourier-Transform infrared (FTIR) spectroscopy, and electron probe microanalysis (EPMA). FTIR analysis gives information about the atomic configuration and distribution of hydrogen and structurally bond water in quartz (*e.g.,* Kats 1962; Bambauer *et al*. 1963; Aines & Rossmann 1984; Kronenberg *et al*. 1986; Rovetta *et al*. 1989; Bahadur 1994). The micro-distribution of the trace elements Al, Ti, K and Fe in quartz is determined by EPMA with a spatial resolution down to 5 µm. This combination of analytical techniques allows a crystal-chemical characterisation of igneous quartz and therewith a better understanding of large-scale magmatic processes.

2. Methods

2.1. Optical microscope cathodoluminescence (OM-CL)

CL spectra and colour images were obtained using a hot-cathode luminescence microscope HC3-LM (Neuser *et al.* 1995). The electron gun operates at a voltage of 14 kV under high vacuum (10^{-5} mbar) and a filament current of 0.18 mA resulting in a current density of ca. 10 mA/mm^2 at the sample surface. Photographic documentation was carried out with a NIKON Microflex UFX-II system equipped with a NIKON FX-35A reflex camera.

The spectral response of the luminescence was recorded with a triple-grating (100 lines/mm, 1200 lines/mm, and 1800 lines/mm) spectrograph TRIAX 320 equipped with a LN$_2$-cooled CCD-detector. The 100 lines/mm grating was used to acquire emission spectra in the range of 400 - 900 nm (3.1 - 1.4 eV); the 1200 lines/mm grating corresponds to a spectral range of 70 nm. The CL-emission was collected for an area of ~0.5 mm^2 using a 20x/0.40 objective. The integration time for spectrum acquisition was 20 s for the 100 lines/mm grating and 30 s for the 1200 lines/mm grating. The spectra were corrected for the total detector response. The CL emission spectra are presented as the sum total of Gaussian curves for the different emission lines. These spectra have been deconvoluted using the procedure of Müller *et al.* (2002b). The time-dependent variations of the 1.96 and 2.79 eV emission-line intensities during electron radiation were recorded with a f/3.4 Grating Monochromator at a speed of 10 mm/min.

2.2. Scanning electron microscope cathodoluminescence (SEM-CL)

Two scanning electron microscopes equipped with different CL detectors, the Cambridge Instruments 250-MK3 with a S20-Extended photomultiplier and the JEOL JXA 8900 with a CLD40 R712 photomultiplier, were used for the study of microtextures in quartz. The detectable wavelength for both photomultipliers ranges from 380 to 850 nm (3.26 – 1.46 eV). SEM-CL allows a better spatial resolution down to 1µm^2 and the capability of combining CL with back scattered electron (BSE) imaging and electron microprobe analysis (EPMA). The possibility of increasing the power density over small sample areas is useful for samples with low CL intensity. A disadvantage is the monochromatic (grey scale) image. Weakly luminescing quartz corresponds commonly to red to reddish brown CL and bright quartz to blue to violet colours, with the present instrument. Images were collected from the JEOL system using a beam voltage of 30 keV, a filament current of 200 nA, slow beam scan rates of 20 s at processing resolution of 1024x860 pixels and 256 grey levels. The voltage and sample current for the Cambridge Instruments 250-MK3 was 20 keV and 5-15 nA, respectively. The documentation of the CL images at the 250-MK3 were carried out with a photo camera with

4

Agfapan APX 25 films and by using slow beam scan rates of 250 sec. The contrast of the images was improved by using the software PhotoShop for Windows.
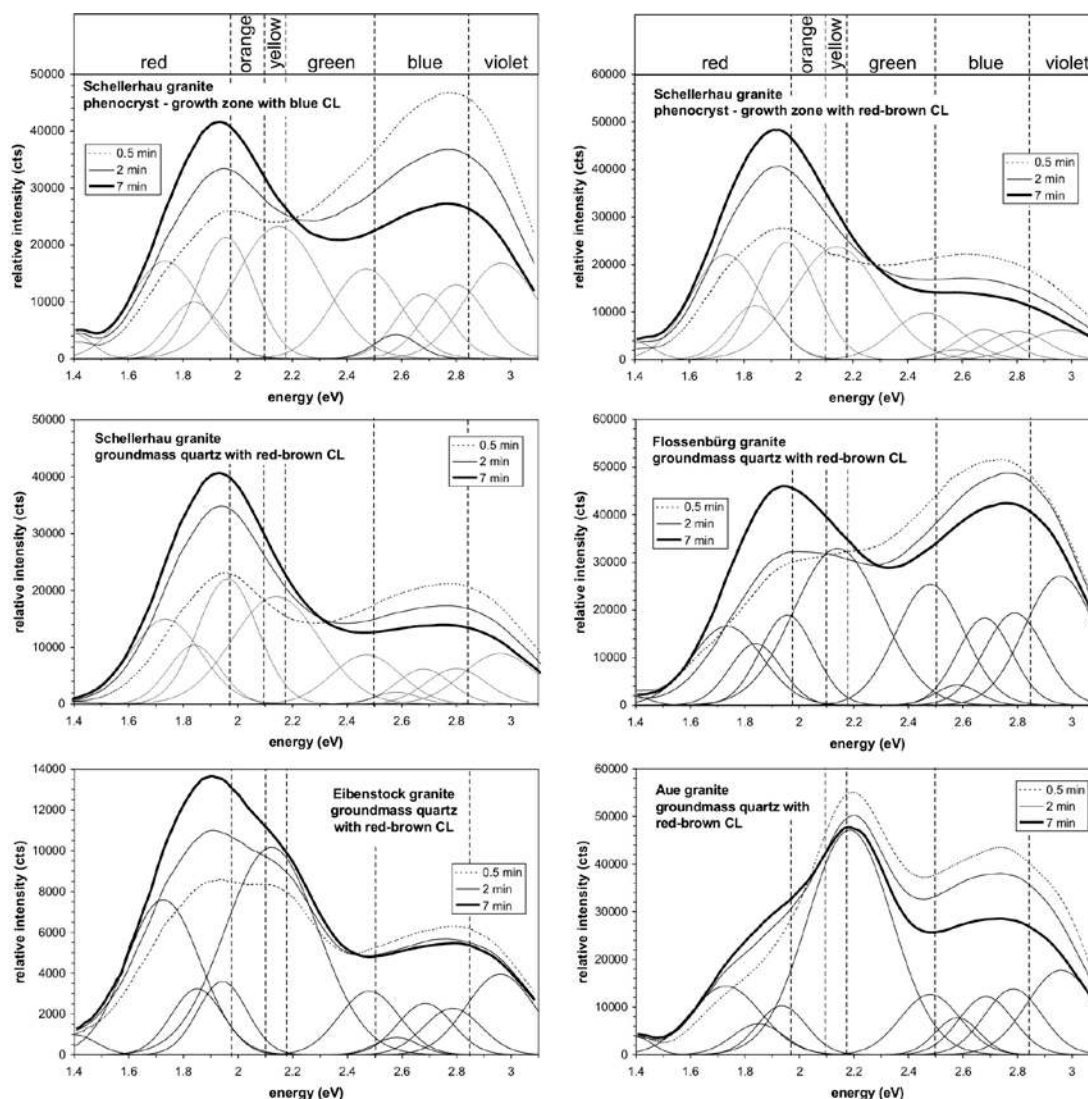

Figure 2 CL spectra of igneous quartz recorded with the 100 lines/mm grating after 30 s, 2 and 7 min of electron bombardment. The 7-min-spectra were resolved by best fitting with Gaussian curves.

2.3. Electron probe microanalysis (EPMA)

Trace element abundances of Al, K, Ti, and Fe in quartz were performed with a JEOL 8900 RL electron microprobe with 5 wavelength dispersive detectors at the Geowissenschaftliches Zentrum Göttingen. Synthetic Al_2O_3 (52.9 wt.% Al), orthoclase from Lucerne, Switzerland (12.2 wt.% K), synthetic TiO_2 (59.9 wt.% Ti), and haematite from Rio Marina, Elba (69.9 wt.% Fe) were used for standards. A beam current of 80 nA, an accelerating voltage of 20 kV, diameter of 5 µm, and counting times of 15 s for Si, and of 300 s for Al, Ti, K, and Fe were used. Raw analyses were converted into concentrations using the phi-rho-Z matrix correction method of Armstrong (1995). Analytical errors were calculated from the counting statistics of peak and background signals, following the Gauss law of error propagation. At low element concentrations the background forms the main part of the total signal. On the other hand, the background signal is nearly constant for a given quartz matrix and the absolute error based on

5

counting statistic is thus nearly constant. Limits of detection by single measurement average (3σ; n = 36) are 13 ppm for Al, 13 for Ti, 10 for K, and 15 for Fe.
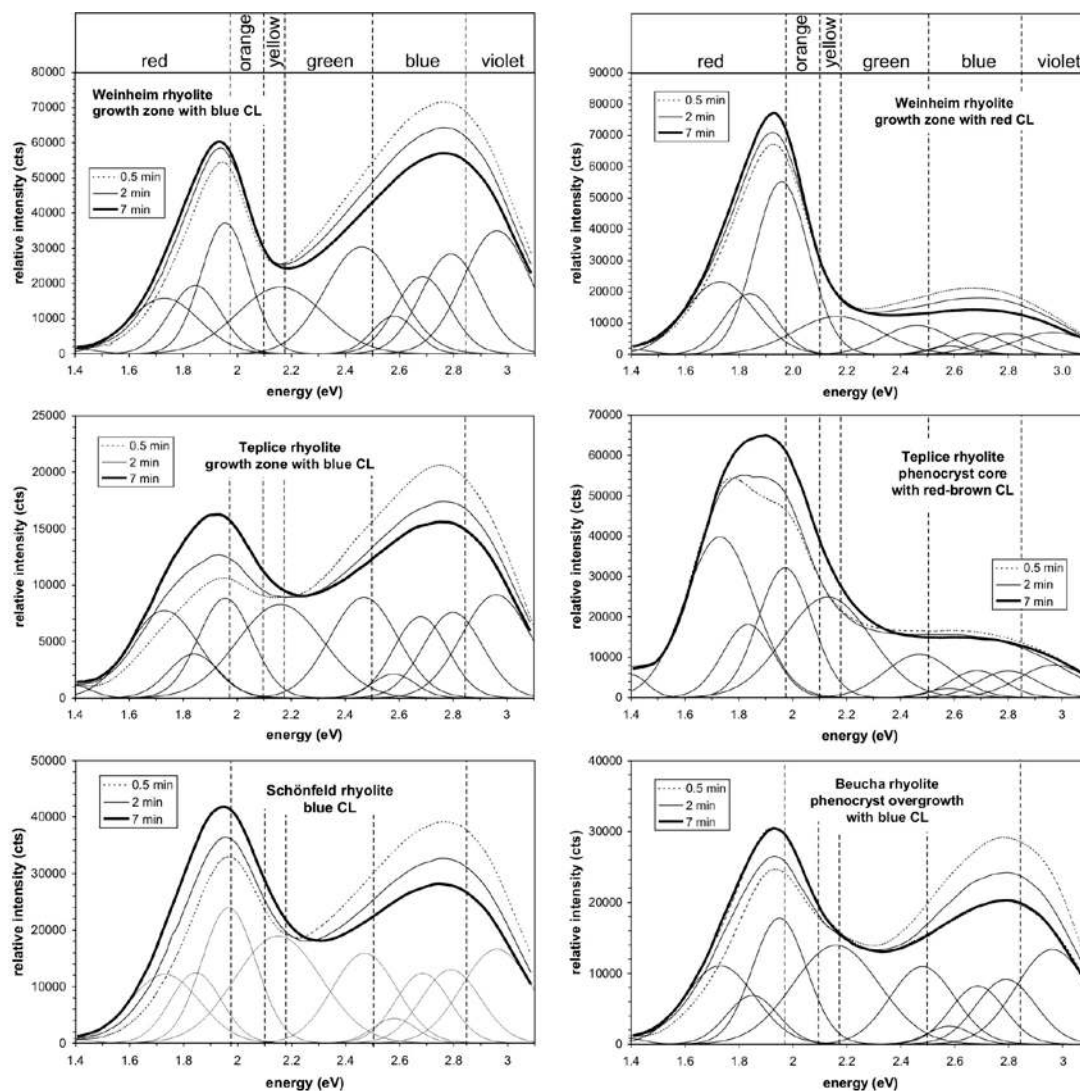

Figure 2 (Continued)

2.4. FTIR spectroscopy

Infrared analysis was performed at the GeoForschungsZentrum Potsdam using a Bruker IFS 66v FTIR-spectrometer coupled with an IR-microscope (Hyperion 1000). The measurements were performed in-situ at –190 °C using a Linkam FTIR600 heating/freezing stage. The spectra were acquired from 4500 to 2500 cm^{-1} with a resolution of 2 cm^{-1}. Analyses were carried out on doubly-polished wafers of quartz crystals (diameter about 3 mm) with a thickness of 50 - 80 µm. The beam diameter on the sample ranged from 30 to 40 µm and allows the detection of variations within individual quartz crystals. 4 to 8 points along a line in one crystal could be measured. We used thin quartz wafers to minimize the risk of encountering fluid inclusions, which are common in quartz from subvolcanic and plutonic rocks. Prior to the analysis the wafers were cleaned with acetone and dried for 10 h at 110°C. The spectra were corrected for the wafer thickness.

3. Cathodoluminescence of igneous quartz

6

The cathodoluminescence of igneous quartz shows commonly shades of blue, violet, red and red-brown. These colours mainly result from emissions in the red (1.7 – 2.2 eV) and blue (2.4 – 3.1 eV; Fig. 2). Contrary to most other luminescing minerals, the defect structure inventory of quartz, and therewith the cathodoluminescence, is influenced by the electron beam. The ratio of the red and blue emission ranges changes with the irradiation time, whereby the blue emission normally decreases and the red emission increases (Fig. 2). As a consequence, the initial CL signal is difficult to detect. The radiation damage of the upper ca. 5 µm of the quartz sample surface means that the luminescence is non-reproducible.

High-resolution spectral analysis shows that both red and blue emissions are composed of several emission lines. Three emission bands are distinguished in the red emission range (1.73, 1.84, and 1.96 eV), and five bands in the blue emission range (2.47, 2.58, 2.68, 2.79, and 2.96 eV). A broad yellow band has been identified at 2.15 eV (Table 1; Fig. 2). The individual CL emission bands can be localised and quantified from best-fit Gaussian curves by working out about ca. 100 spectra (Müller 2000). The CL band positions are reported also in the literature (*e.g.,* Remond *et al.* 1992; Gorton *et al.* 1996; Steven Kalceff *et al.* 2000 and references therein; Table 1).

Table 1 Detected CL emission bands of igneous quartz (1.4 – 3.1 eV) and their possible association with trace elements and defect centres according to literature.

Band position (eV)	Half width (eV)	Proposed origin	Reference with band position
1.73±0.02	0.3±0.02	substitutional Fe^{3+}	Pott & McNicol (1971) – 1.78 eV
			Kempe *et al.* (1999) – 1.75 eV
1.84±0.01	0.22±0.01	nonbridging oxygen hole centre	Sigel & Marrone (1981) – 1.85 eV
1.96±0.02	0.22±0.02	oxygen vacancy	Luff & Townsend (1990) – 1.91 eV
		nonbridging oxygen hole centre with OH^- groups as precursors	Stevens Kalceff & Phillips (1995) - 1.95 eV
2.15±0.02	0.38±0.01	E' center $[SiO_3]^{3-}$	Götze *et al.* (1999) - 2.1 eV
		associated with substitutional Ge	Luff & Townsend (1990) – 2.18 eV
2.47±0.02	0.30±0.03	extrinsic defect	Stevens Kalceff & Phillips (1995) – 2.46 eV
		$[GeO_4/Li^+]^0$	Götze *et al.* (2005) – 2.45 eV
2.58±0.01	0.18±0.005	intrinsic defect	Gritsenko & Lisitsyn (1985) – 2.58 eV
2.68±0.01	0.23±0.01	self trapped exciton combined with E' center $[SiO_3]^{3-}$	Stevens Kalceff & Phillips (1995) – 2.68 eV
2.79±0.01	0.26±0.01	self trapped exciton	Itoh *et al.* (1990) – 2.8 eV
2.96±0.015	0.30±0.02	intrinsic defect	Stevens Kalceff & Phillips (1995) – 2.93 eV
		associated with substitutional Ti	Müller *et al.* (2002b) – 2.96 eV

The blue 2.68 and 2.58 eV bands have a constant band area ratio of 1 : 0.34±0.08. Similar observations were made for the red 1.96 and 1.84 eV bands, which show a ratio of 1 : 0.51±0.17. Predominant emission bands of zoned quartz phenocrysts are the 1.96, 2.58, 2.68, 2.79, and 2.96 eV band. Exceptions are the phenocrysts from the Eibenstock and Aue granite from the Western Erzgebirge, which show a characteristic 2.15 eV emission. Some growth zones in the phenocrysts show a marked 1.73 eV emission. The growth zones within quartz phenocrysts correspond to variable intensity of the blue emission, whereas the red emissions are approximately constant.

The blue emission (2.6 – 3.1 eV) shows high intensity at initial electron bombardment, but a part of the blue emission lines mostly centred at ~2.8 eV (2.58, 2.68, 2.79 and 2.96 eV), drop by 1/2 to 1/3 after a few seconds. However, the 2.79 eV emission decreases much more than the 2.58, 2.68 and 2.96 eV emissions (Müller 2000). After 30 to 100 s of electron

bombardment the CL is stabilised, pointing at a constant number of luminescence centres at the experimental conditions. The applied experimental conditions resulted in a beam current density of ~10 mA/mm^2 at the sample surface and temperature increase of ca. 110°C during 100 s initial bombardment. The red emissions (1.75 – 2.2 eV) show lowest intensity at initial electron bombardment followed by a steep parabolic increase during the first minute of electron radiation followed by a slight increase until a stable luminescence is reached.

Most of the energy of the electron beam is transformed into heat in the sample (*e.g.,* Remond *et al*. 1992). By using the present equipment, the temperature of the sample may increase by up to 140°C after 10 minutes of electron beam irradiation (Müller 2000). Therefore, thermoluminescence bands may impose CL spectra. Characteristic thermoluminescence bands are at 2.95-2.85 eV, 2.21-2.14 eV and 2.00-1.98 eV (*e.g.,* Jani *et al.* 1983; Rink *et al.* 1993; Yang *et al.* 1994). The intensity maxima of the 2.21-2.14 eV and 2.00-1.98 eV bands lie in the temperature range of the CL measurements. However, the marked different CL for different quartz types in the same temperature range demonstrates that the effect of temperature is relatively small (Müller 2000).

The kinetic law $c = c_0 \exp(-kt)$ (c = concentration of the component at time t, c_0 = concentration of the component at time t = 0, and k = velocity [equilibrium] constant) has been applied in order to quantify the changes of CL during electron beam irradiation (Ramseyer *et al.* 1988; Picouet 1999); the increase of the red CL can be described by the reverse equation of the kinetic law. In this way, the CL intensity can be approximately quantified as a function of time. According to Ramseyer *et al.* (1988) and Picouet (1999) the fastly decaying component and the slowly decaying components in the blue CL-range are calculated as the sum of two kinetic law equations:

$$I_b = I_{bs} + I_{b1} * \exp(-t/k_{b1}) + I_{b2} * \exp(-t/k_{b2}) \qquad (1)$$

where I_b = intensity of blue CL at the radiation time t; I_{bs} = intensity of stable blue CL; I_{b1} = intensity of the slow decreasing CL component at t = 0; k_{b1} = velocity constant of the slow decreasing CL component; I_{b2} = intensity of the fast decreasing CL component at t = 0; k_{b2} = velocity constant of the fast decreasing CL component; t = radiation time.

The increase of red emission can be described by the equation:

$$I_r = I_{rs} - I_{r1} * \exp(-t/k_{r1}) - I_{r2} * \exp(-t/k_{r2}) \qquad (2)$$

where I_r = intensity of red CL at the radiation time t; I_{rs} = intensity of red CL for $t \to \infty$; I_{r1} = intensity of the slow increasing CL component for $t \to \infty$; k_{r1} = velocity constant of the slow increasing CL component; I_{r2} = intensity of the fast increasing CL component for $t \to \infty$; k_{r2} = velocity constant of the fast increasing CL component; t = radiation time.

The velocity constants k_{r1}, k_{r2}, k_{b1}, and k_{b2} depend on the measurement conditions and are similar for the present samples. Müller (2000) showed that for different quartz types the decay of the luminescence centres causing blue CL is about 2 times faster than that of those causing red CL. The emission intensities (I) correspond to the concentration of luminescence centres in the interaction volume of the electron beam. The parameters I_{rs}, I_{r1}, I_{r2}, I_{bs}, I_{b1}, and I_{b2} are the intensity portions of all emissions, whereby I_{r1}, I_{r2}, I_{b1}, and I_{b2} are intensity portions of the changeable CL. In granites, zoned quartz phenocrysts have low I_{r2} and I_{b2}, which is indicative of more stable defect structures compared to the groundmass quartz (Fig. 3). The latter quartz exhibits widely varying intensities reflecting a high concentration of unstable defect

structures. The high I_{r1} and I_{r2}, which is characteristic for granitic groundmass quartz, demonstrate the predominance of unstable red CL.
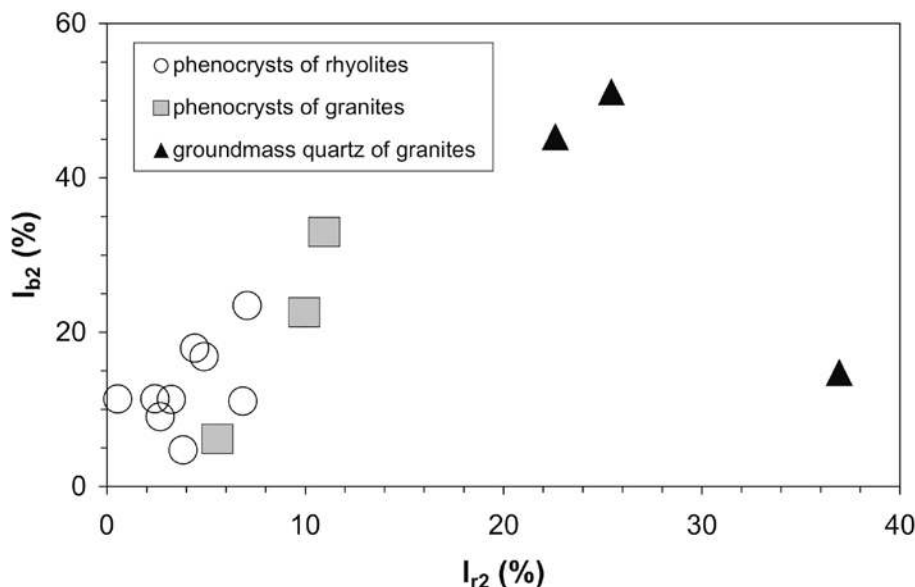

Figure 3 Plot of the of fitted parameters I_{r2} and I_{b2} representing fast changing CL components of the red CL (1.96 eV) and blue CL (2.79 eV), respectively. Granitic groundmass quartz exhibit the most unstable CL characterised by a strong increase of the red CL.

4. Intra-granular textures of igneous quartz

4.1 Primary growth textures

The term "primary growth textures" is used here for intra-granular growth patterns which develop during crystal growth in the magma; secondary structures are the result of alteration.

Primary growth textures may develop in (1) early-magmatic quartz phenocrysts, (2) late snowball quartz in highly evolved albite granites (*e.g.,* Müller & Seltmann 1999), and (3) comb quartz in layered granitic rocks (*e.g,* Müller et al. 2002a).

4.1.1. Early-magmatic quartz phenocrysts

Quartz phenocrysts have been described worldwide from rhyolites, rhyodacites and some dacites with ≥ 63 wt.% SiO_2. In dacites or other more mafic volcanic rocks quartz phenocrysts are commonly rounded and sometimes show coronas of hornblende, pyroxene and/or An-rich plagioclase (oscelli texture) indicating disequilibrium with the melt (*e.g.*, Mashima 2004). They must have been inherited from a more felsic magma prior to emplacement or extrusion.

Phenocrysts in volcanic rocks can be easily recognised due to the grain size contrast between them and the micro- to fine-crystalline groundmass. However, groundmass minerals in plutonic rocks are coarser grained and may overgrow phenocrysts. The early magmatic crystals may be not phenocrysts in the strict sense because they may not have shared common histories and crystallised from a melt in which they are now hosted, but rather represent a melt laced with a crystal cargo that has been inherited from melts that existed at different places and times in the magma system (Davidson *et al.* 2007). Neither are they strictly xenocrysts, as they are grown and recycled from closely related progenitor magmas rather than accidentally incorporated from unrelated wallrocks. W.E. Hildreth (personal communication in Davidson *et al.* 2007) suggested the term "antecryst" to denote phases that originate in the magma

9

system, but are not true phenocrysts (*cf* Charlier *et al.* 2005). Davidson *et al.* (2007) proposed that magmatic rocks can be represented by mixtures of melts, recycled antecrysts, and true phenocrysts. However, in this study the dominant early magmatic crystal populations of grantic rock are discussed and, therefore, they are considered as true phenocrysts.
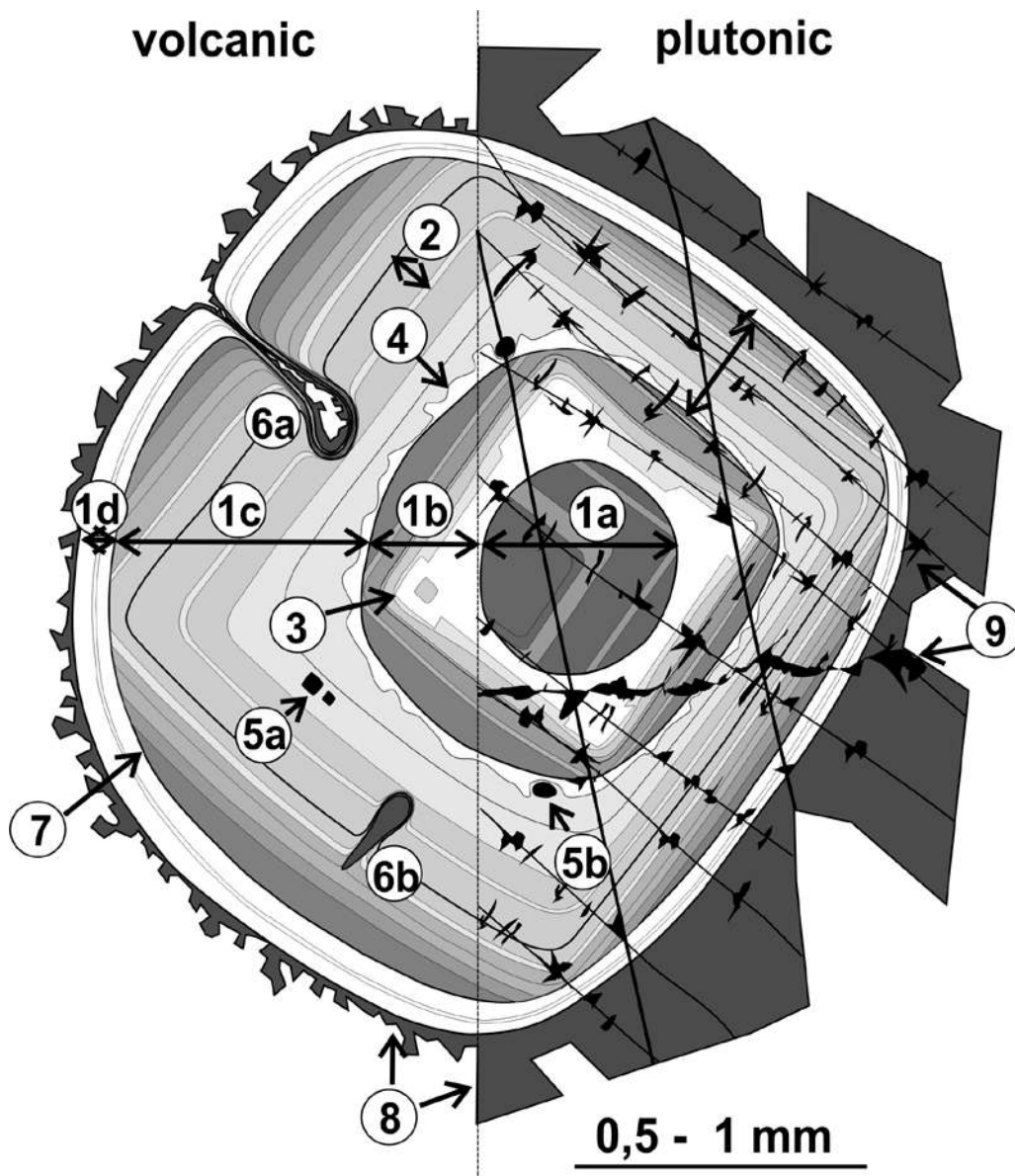

Figure 4 Schematic illustration of growth textures observed in early-magmatic quartz phenocrysts of late-Hercynian felsic igneous rocks. 1a-d – step zones, 2 – oscillatory zone, 3 – skeletal growth, 4 – wavy surface, 5a – melt inclusion with negative crystal shape, 5b – ovoid melt inclusion, 6a – lobate growth embayment, 6b – closed growth embayment, 7 – resorption surface, 8 groundmass quartz, 9 –secondary structures.

In plutonic rocks phenocrysts are often difficult to identify, but can be identified by their contrasting CL. The majority of the late-Hercynian granites with ≥ 65 wt.% SiO_2 contain quartz phenocrysts (Müller *et al.* 2000, 2002a, 2003b, 2005, 2006a; Table 2). In some granites the phenocrysts comprise a substantial part of the rock up to 40 vol.% (*e.g.,* Müller *et al.* 2000), whereas in other granites phenocrysts are rare or even absent. A number of late-Hercynian granites with ≥ 63 wt.% SiO_2 contain exclusively anhedral groundmass quartz without zoning, *e.g.* the Flossenbürg and Leuchtenberg granite from the Oberpfalz.

Groundmass quartz may show euhedral crystal cores with brighter CL, *e.g.* Rozvadov granite, Oberpfalz. Migmatitic granites, chemically highly evolved albite granites and fluid-enriched aplites and miarolitic granites are generally free of early-magmatic quartz phenocrysts.

The development of zoning in phenocrysts requires that the quartz grew in an evolving magma reservoir. Microscopic growth zone boundaries represent relic crystal-melt interfaces, which develop by fluctuations of growth and diffusion rates. The zoning pattern of the phenocrysts is normally more complex in granites and rhyolites with high SiO_2 content (>70 wt.%). This can be explained by the early SiO_2 saturation with the consequence of a longer period of quartz precipitation prior to final magma emplacement or extrusion. Phenocrysts in granites and rhyolites show similar growth patterns. In some cases, quartz phenocryst populations in granites are similar to populations in the associated rhyolites (*e.g.,* Schellerhau granite and Teplice rhyolite; Müller *et al.* 2005). However, the zoning of granitic phenocrysts is normally less well developed. The zoning may have been quenched or overprinted during slow magma cooling and be destroyed by the interaction with deuteric fluids.
Growth patterns in quartz of granites and rhyolites have been described in Müller *et al.* (2000, 2003b, 2005). We distinguish fine-scale (2-20 µm) oscillatory zoning, large-scale step zoning (compositional zoning), skeletal growth, wavy and resorption surfaces and growth embayments (Fig. 4).

The SEM-CL images of Figures 5 and 6 display characteristic growth textures in igneous quartz from late-Hercynian granites and rhyolites from Central Europe. The images represent a selection of about 1400 pictures taken from more than 260 thin sections. The examples in Figures 5 and 6 represent common features in these rocks. Each igneous system has its own distinctive fingerprint as recorded in the zoning pattern (Table 2).

Textures indicate that epitaxy must be important for quartz nucleation. Quartz nucleates on tiny grains of feldspar, mica, accessory minerals, or on immiscible melt droplets or bubbles occasionally preserved as melt inclusions (Figs. 5b, c). Sometimes two or more quartz crystals grow around one particle. Particularly in granites these crystals may coalesce to become one crystal or they grow separately forming clusters of 2 to 5 crystals (Fig. 5b). Phenocrysts nucleate commonly as dihexagonal β-quartz. Rhombohedral α-quartz has been described by Flick (1987) from rhyolites from the Odenwald. Phenocrysts from the Odenwald show skeletal overgrowths in their cores (Fig. 5c). Skeletal growth reflects a kinematically driven, non-equilibrium growth phase (*e.g.,* Kirkpatrick 1981; Fenn 1986; Fowler 1990) which is in accordance with the undercooling experiments of Fenn (1977) and Swanson (1977), who showed that growth is controlled by diffusion during rapid crystallization.

Correlative zoning patterns of quartz phenocrysts from the same magma batch indicate that the crystals of one population nucleated simultaneously and continued growing together (Peppard *et al.* 2001; Müller *et al.* 2000, 2005). Some rocks contain two or more phenocryst populations, whereby one population dominates. Each population represents one nucleation event. In this way the temporal crystallisation history of a magma batch can be reconstructed (Müller *et al.* 2000). Due to multiple magma recharge quartz populations with a different history can be mingled (Müller *et al.* 2005). This is known from plagioclase in mafic and intermediate rocks (*e.g.,* Davidson *et al.* 2001). The first growth stage of quartz phenocrysts may be interrupted by resorption resulting in rounding of the crystal nuclei. The resorption surface truncates pre-existing growth zones and results in the rounding of crystals.
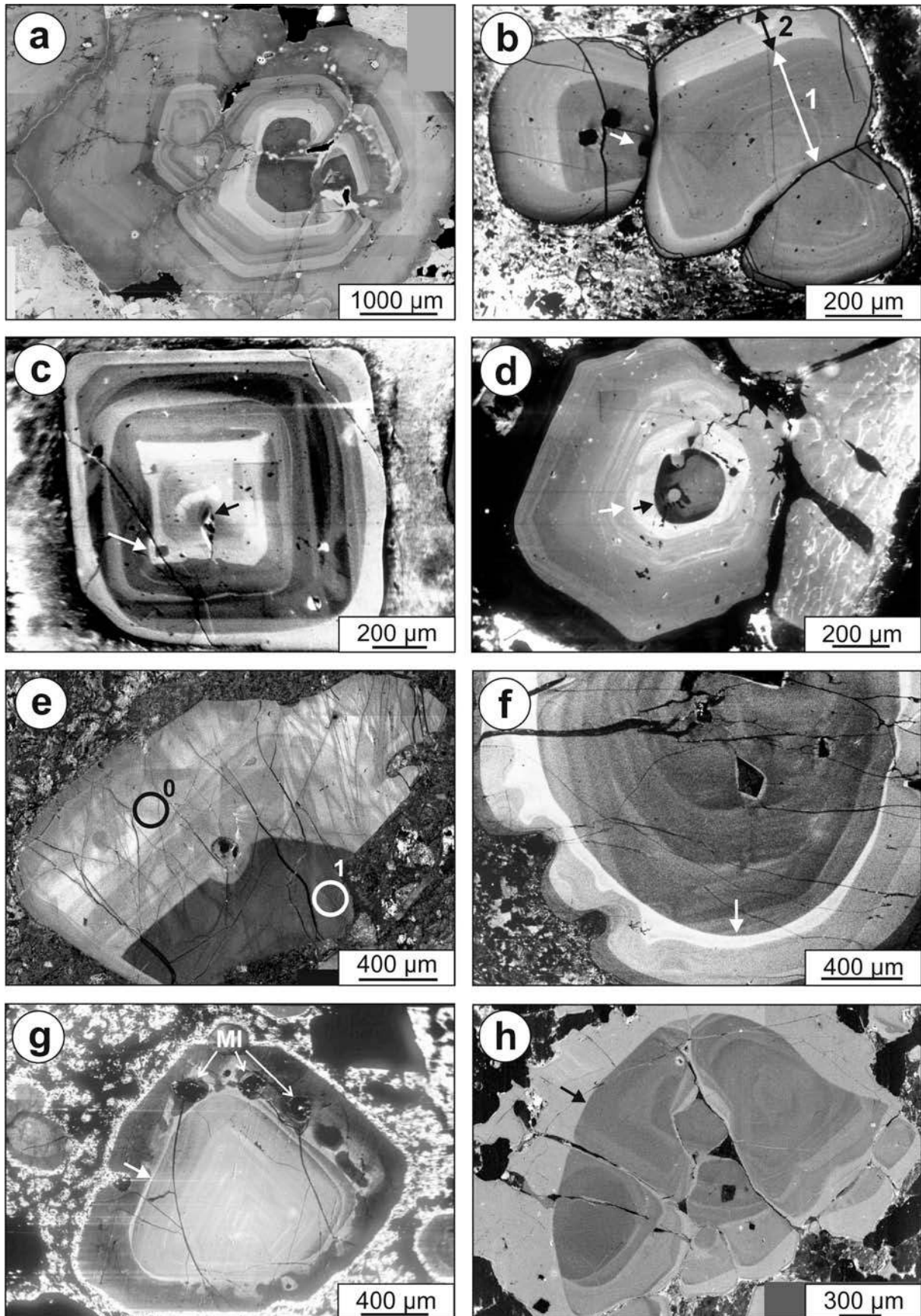
Figure 5 SEM-CL images of early-magmatic quartz phenocryst from late-Hercynian felsic igneous rocks illustrating the variability of primary growth textures. a – Zoned quartz phenocryst embedded in groundmass quartz. Schellerhau granite SG2. b - Cluster of three zoned phenocryts of the Gattersburg rhyolite (NW Saxony, Germany). The left crystal germinated at melt droplet which is now preserved as melt inclusion (white arrow). The growth pattern is characterised by two step zones with subordinate oscillatory zoning. The relatively homogenous pattern indicates almost undisturbed crystal growth. The phenocrysts show several thin healed contraction cracks (black) caused by shock cooling during eruption. c – Rhyolitic phenocryst with α-quartz habit with complex growth pattern (Dossenheim, Odenwald). The bright crystal core, which germinates at a melt/volatile droplet (black arrow), shows skeletal growth (white arrow). d – Rhyolitic phenocryst (Hengstberg, NW Saxony) with dull luminescing, resorbed crystal core (black arrow) with bright overgrowth (white arrow). The euhedral phenocryst is overgrown by almost non-luminescing groundmass quartz (black). e - Fracture of zoned phenocryst with weak luminescing core (Teplice rhyolite, Erzgebirge). Circles correspond to FTIR absorption sampling spots. f - Rhyolitic phenocryst (Fichtelgebirge) with a major resorption surface (white arrow). Subsequent wavy growth show bright luminescence. g - Rhyolitic quartz phenocryst (drill core KB1 Wittichen 263-264 m, Black Forest). The resorption event (white arrow) is followed by irregular growth which result in the entrapment of numerous large melt inclusions (MI). h – Phenocryst of the Beucha granite porphyry (NW Saxony). The resorbed cluster of zoned phenocrysts (black arrow) is embedded in bright luminescing anhedral groundmass quartz.

This process is recorded by rounded crystal cores with weak red-brown CL as commonly found for the Eastern Erzgebirge granites and rhyolites (Figs. 5a, d).

Major resorption surfaces are typically overgrown by bright blue luminescing quartz (Müller *et al.* 2003b). Sometimes the blue luminescing overgrowth is very thin (<10 µm) and may show a dendritic or wavy structure (Figs. 6a). These overgrowths may be enriched in ovoid melt inclusions (Figs. 5g).

Fine-scale (1-5 µm) oscillatory growth zones with low amplitude in CL are sometimes separated by zones recording resorption or skeletal overgrowth, accompanied by a major change of the CL properties. These events with high-amplitude CL superimpose on the oscillatory zoning. Growth stages of low amplitude CL bordered by resorption or skeletal growth are considered step zones (Fig. 5b; Allègre *et al.* 1981). Analogous distinction between low-amplitude (An-content) fine-scale zoning and superimposed high-amplitude large-scale zoning has been made for plagioclase phenocrysts (Pearce & Kolisnik 1990). The quartz phenocryst of Fig. 5b shows 2 step zones. The definition of step zones becomes more complicated for phenocrysts with complex growth patterns. For example, 6 step zones can be distinguished in the phenocryst shown in Fig. 5c.
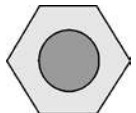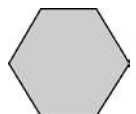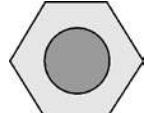
4.1.2. Late-magmatic snowball and comb quartz

Highly evolved topaz-bearing albite granite contains typically so-called snowball quartz (Beus *et al.* 1962; Kovalenko 1977; Sonyushkin *et al.* 1991; Poutiainen & Scherbakova 1998; Müller & Seltmann 1999; Müller *et al.* 2002a; Figs. 6b, c). These rocks occur in the apical part of sub-volcanic granite complexes and are commonly associated with rare-metal mineralisation. Snowball quartz has a dull red-brown to bright red/orange CL, in contrast to early-magmatic quartz phenocrysts, which have predominantly bluish to violet CL. The crystals show gradual transitions into the ramified dendritic crystal margin and into the matrix quartz without changes of the CL properties. Older quartz generations, which may be present in the albite granites are cannibalised by snowball quartz as shown in Fig. 6c. Inclusions of groundmass minerals, such as corroded K-feldspar, mica, zircon, apatite and particularly albite are enriched in the growth zones. Fluid and melt inclusions are abundant throughout the snowball quartz. Lath-shaped albite crystals wrap around the snowball quartz indicating that the quartz pushed aside the albite laths during growth in a dense crystal mush. The snowball quartz shows oscillatory growth zoning with low CL contrasts. The zone boundaries are characterised by planar growth zones with α-quartz crystal habit. Resorption surfaces, which

are characteristic for early-magmatic phenocrysts, have not been observed in the snowball quartz.

Comb quartz occurring typically in granitic line rock nucleates at intra-granite contacts (Breiter *et al.* 2005). It has similar CL properties and structural features as the snowball quartz with the difference that it does not form double-ended crystals (Fig. 3c in Müller *et al.* 2002a).

Table 2 Characteristic features of quartz phenocrysts in late-Hercynian igneous rocks.

late-Hercynian igneous province	investigated igneous rocks	rock type	SiO$_2$ wt.%	characteristic growth structures of phenocrsyts	schemes of growth structures of dominant phenocrsyt populations (oscillatory zoning is not shown)
Eastern Erzgebirge	Eastern Erzgebirge volcano-plutonic complex	granodiorite, monzogranite, rhyodacite, rhyolite	69-75	phenocryst with complex, contrast-rich zoning, low CL rounded crystal cores, Ti-rich margin (reverse zoning), zoning with β-quartz habit (Figs. 2a, e, 7a, d, e)	
Western Erzgebirge	Eibenstock Nejdek pluton	monzogranite	68-78	phenocrysts with complex, contrast-poor zoning, zoning with β-quartz habit	
Oberpfalz	Rozvadov, Leuchtenberg, Flossenbürg, and Falkenberg granites	tonalite, diorite, redwitzite, granodiorite, monzogranite	52-76	no phenocryst or phenocrysts with simple, contrast-poor zoning, zoning with β-quartz habit	
Odenwald	Weinheim, Dossenheim	rhyolite	71-74	phenocryst with complex, contrast-rich zoning, skeletal growth, zoning with α-quartz habit (Figs. 2d, 7e)	
Cornwall	Land's End granites	granite	66-77	phenocrysts with contrast-poor zoning, zoning with β-quartz habit	

4.2 Secondary CL structures

Secondary structures in the CL observation mode are principally formed by five processes: 1) micro-cataclasis followed by healing, 2) stress-induced and fluid-driven quartz dissolution and precipitation, 3) stress-induced lattice reorganisation (purification), 4) impurity element diffusion, and 5) α-radiation.

In a cooling magma late- to post-magmatic fluids may result in small-scale quartz dissolution-precipitation along grain boundaries and micro-fractures. Dense healed fractures connecting low-luminescing domains around fluid inclusions are widespread in granitic rocks (Sprunt & Nur 1979; Behr & Frentzel-Beyme 1989; Valley & Graham 1996; D'Lemos *et al.* 1997; Van den Kerkhof & Hein 2001, Van den Kerkhof *et al.* 2001, 2004; Müller *et al.* 2000, 2002b; Rusk & Reed 2002; Figs. 6a, i, j). Micro-fracturing can be attributed to internal
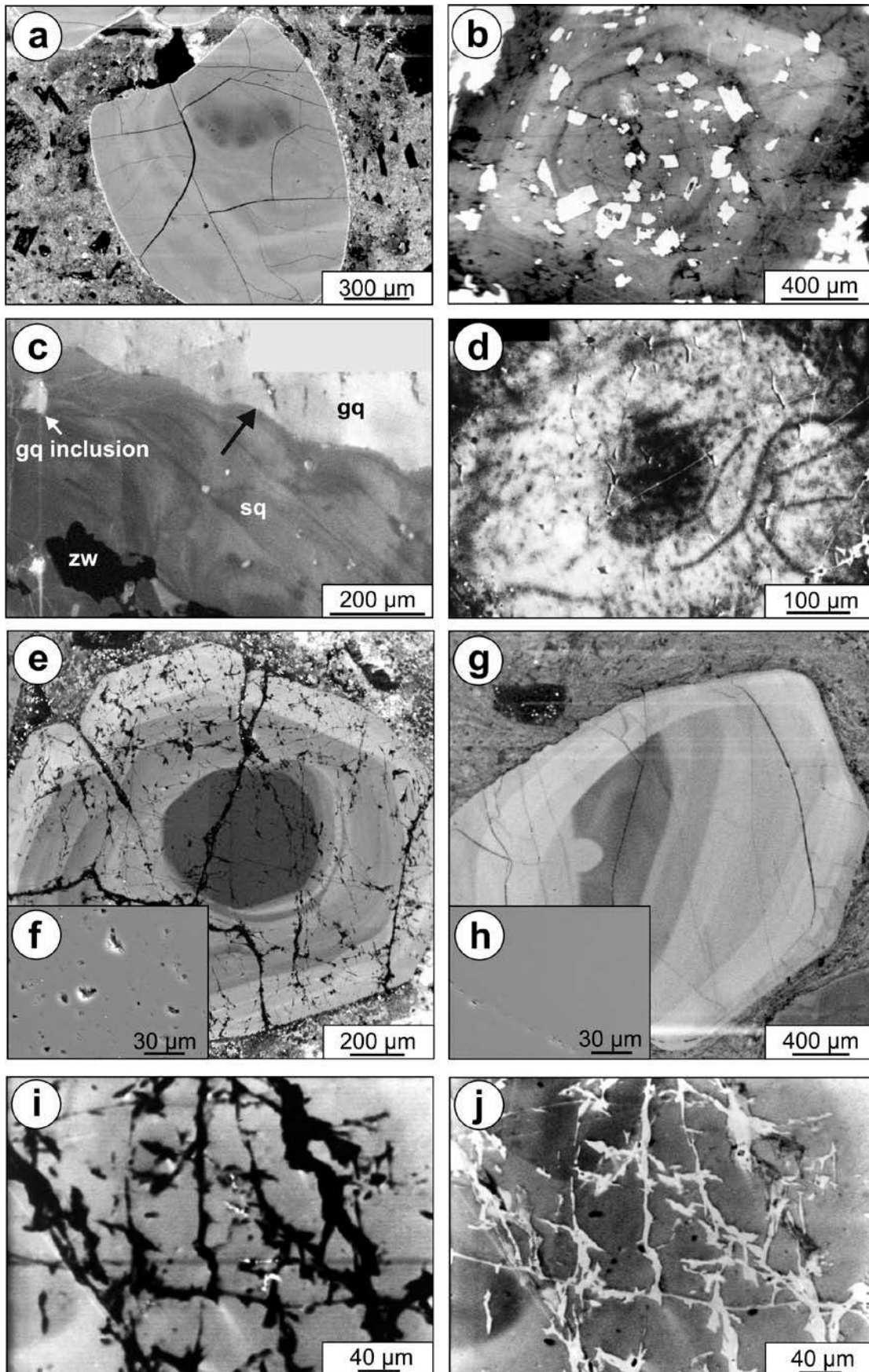
Figure 6 SEM-CL images of quartz in igneous rocks illustrating the variability of secondary structures in early-magmatic quartz phenocryst and textures of late-magmatic groundmass and snowball quartz. a – Rounded (resorbed) quartz phenocryst of the Schönfeld rhyodacite (Eastern Erzgebirge). The internal growth zoning is blurred. The crystal is overgrown by a very thin layer of bright luminescing (white) dendritic groundmass quartz. b – Snowball quartz of the Schellerhau granite SG3, Erzgebirge, with numerous albite inclusions. c – Snowball quartz (sq) cannibalising (white arrow) groundmass quartz (gq) in the Podlesí Dyke granite, Erzgebirge. zw – zinnwaldite. d – Weak luminescing spot-like structures in quartz (Niederbobritzsch granite, Erzgebirge). e - Zoned quartz phenocryst in a subvolcanic rock (Teplice rhyolite TR3c, Erzgebirge). In contrast to (g), the quartz contains a dense network of secondary structures (black). f - BSE image of the surface of (e) with high porosity (up to 2 vol.%). g - Zoned quartz phenocryst from an effusive rock (Teplice rhyolite TR2b, Erzgebirge). h – Back-scattered electron (BSE) image of the quartz surface of (g) showing very low porosity (<0.2 vol.%). i – Network of almost non-luminescing domains and healed cracks in the Schellerhau granite (Erzgebirge) at initial electron bombardment. j - The area shown in (i) after 10 min focused electron bombardment (20 keV, 15 nA). The luminescence of the secondary quartz had been increased drastically.
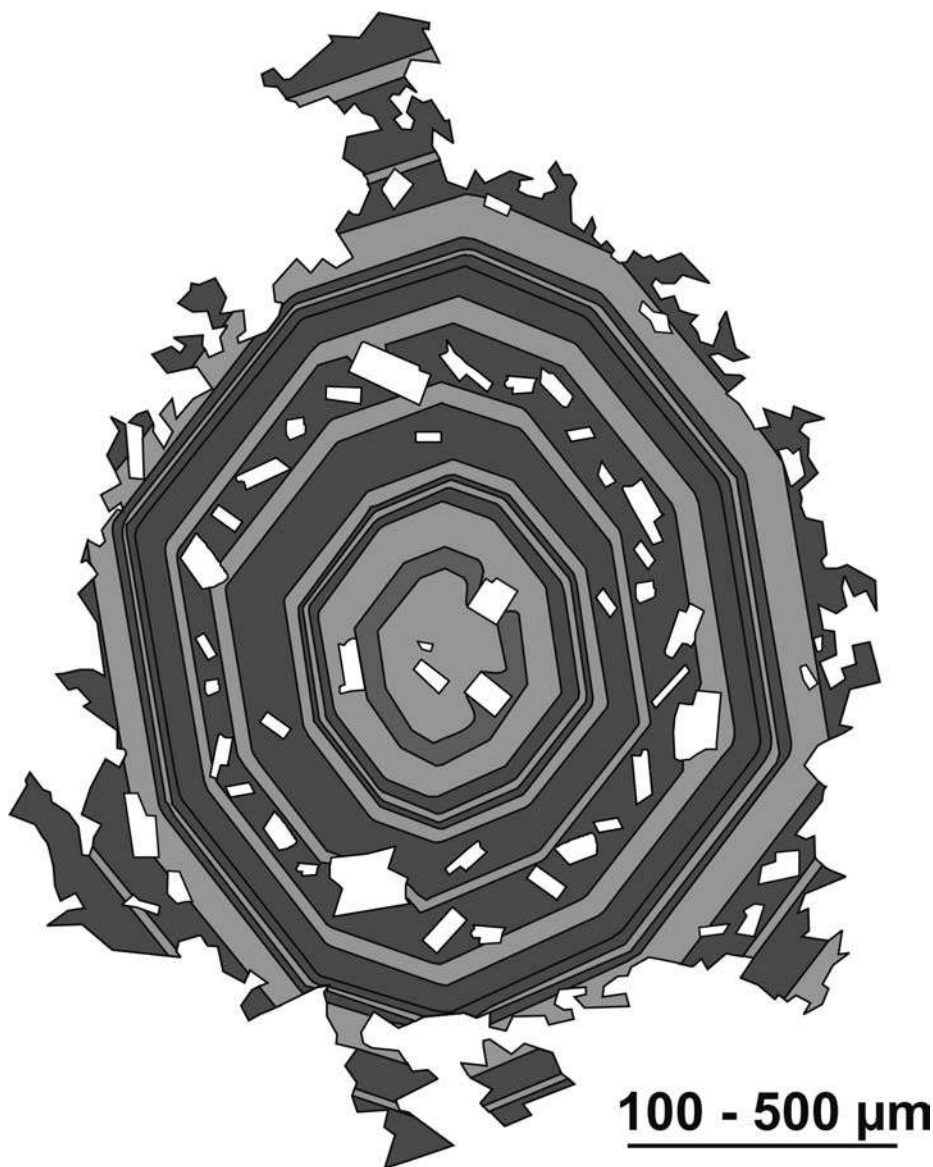

Figure 7 Growth structures of late-magmatic snowball quartz with zonal enclosed albite laths (white). Modified from Müller *et al*. 2002a.

stresses at a grain scale resulting from the thermal contraction of quartz relative to feldspar in the cooling granite (Vollbrecht *et al.* 1991, 1994). The α/β-quartz transformation which causes an anisotropic contraction of 0.86 vol.% vertical to the c-axis and 1.3 vol.% parallel to the c-axis (*e.g.,* Blankenburg *et al.* 1994), imposes additional stress. However, the α/β-quartz transformation is not the dominant process causing the fracture network because these structures are trans-granular meaning independently from crystallographic orientation of the quartz crystals and they are absent in phenocrysts from extrusive rocks (Figs. 6e, g).

Müller (2000), Müller *et al.* (2002) and Van den Kerkhof *et al.* (2004) demonstrated the systematic reduction of Al, Ti and K in secondary quartz compared to the host quartz. However, the CL intensity of secondary quartz may increase after several minutes of electron beam exposure using high beam power densities $>10^4$ W/cm^2 (Figs. 8i, j) resulting in contrast reversal. Partially healed radial and concentric contraction cracks caused by shock cooling are common in quartz phenocrysts from volcanic rocks (Fig. 6a).

Groundmass quartz in granites, which is free of primary growth zoning, commonly exhibits non-luminescing 1-5 µm small micropores, which become visible as dark spots in SEM-CL after several minutes of electron bombardment (Van den Kerkhof & Grantham 1999, Müller 2000, Van den Kerkhof & Hein 2001). Figure 6d shows such spots in quartz from the Niederbobritzsch granite, Eastern Erzgebirge.

Igneous quartz sometimes shows halos of pinkish/yellowish white luminescing quartz around zircon inclusions. These textures are caused by α-radiation damage, i.e. metamictisation of the quartz crystal structure (*e.g.,* Botis *et al.* 2005). The radius of halos is typically about 40 µm. Each halo is subdivided into a brighter inner zone (~25 µm) and an outer zone (~15 µm). The radius of ~40 µm corresponds to the interaction radius of α-particles in quartz (Owen 1988).

5. Trace elements in igneous quartz

Al and Ti are the most abundant trace elements in igneous quartz (Müller *et al.* 2000, 2002a, 2003a, 2003b). The contrasting behaviour of these two elements during magma differentiation make them suitable for discriminating igneous units. Figure 8 shows Al/Ti *versus* Ti discrimination diagrams for igneous quartz from dacites, rhyodacites and rhyolites (Fig. 8a) and from granites (Fig. 8b). Quartz in the most primitive rocks (dacites) has the lowest Al and highest Ti (lowest Al/Ti; Fig. 8a). Ti in quartz decreases and Al increases with progressive differentiation. Ti shows maximum concentrations of up to 130 ppm in the bright blue luminescing growth zones in early-magmatic quartz phenocrysts, whereas the Ti concentration in late-magmatic groundmass quartz in granites shows lower concentrations of 20 to 50 ppm (Müller *et al.* 2002a, 2003a, 2003b). An exponential Al/Ti trend can be recognized (linear trend on the log-log plot of Figure 8), which is however not continuous. The high-Al tails of the data fields of the Schönfeld basal rhyolite, the Teplice rhyolite (Müller *et al.* 2002a) and the rhyolite from Bonne Nuit Bay (Watt *et al.* 1997) are caused by a few out-of-range values (Fig. 8a), which are the result of sub-microscopic inclusions (see chapter 6.1). Taking this into account, Al concentrations in quartz phenocrysts are relatively constant for each volcanic facies, compared to Ti. Al is most variable in evolved granites of the Western Erzgebirge (Podlesí Dyke granite, Aue granite, Slavkov microgranites).

Concentrations of Li, K, Ge, B, Fe, and P in igneous quartz are in the range of 1 to 50 ppm (Schrön *et al.* 1988; Götze *et al.* 2004; Larsen *et al.* 2004; Jacamon & Larsen 2009). All these elements are incompatible and correlate positively with Al, implying that their concentrations increase with progressive differentiation of the magma. Li in quartz may be buffered by Li-bearing micas, which may coexist with quartz at higher degrees of fractionation (Müller *et al.* 2008), whereas B tends to separate into the magmatic vapour

phase (*e.g.,* Pichavant 1981). Secondary quartz is typically depleted in Al, Ti, and K (Van den Kerkhof & Müller 1999; Van den Kerkhof *et al*. 2004; Müller *et al*. 2008).
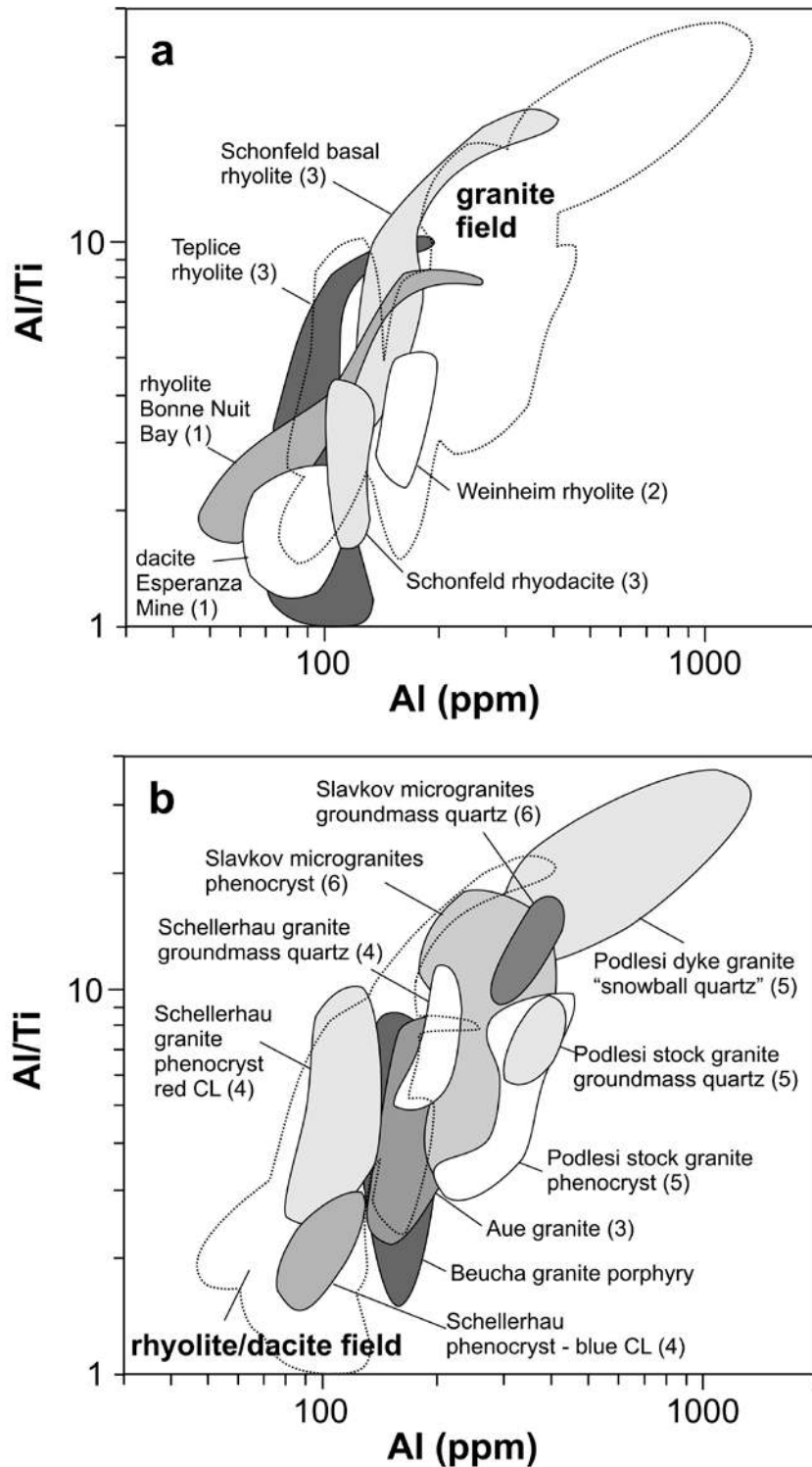

Figure 8 Compilation of Al concentrations and Al/Ti ratios in quartz (a) from dacites and rhyolites and (b) granites. Data were obtained by EPMA and SIMS. (1) Watt *et al*. 1997; (2) Müller *et al*. 2003a; (3) Müller *et al*. 2005; (4) Müller *et al*. 2000; (5) Müller *et al*. 2002a; (6) Müller *et al*. 2003b.

6. FTIR absorption of igneous quartz

The abundance of hydrogen-related defects in igneous quartz has been measured by FTIR spectroscopy. Unpolarized spectra were collected along traverses across quartz crystals (Fig. 9). All spectra show distinct absorption at 3365 cm^{-1} and a minor absorption at 3305 cm^{-1}. Both bands are attributed to hydrogen-compensated Al defects (*e.g.,* Kats 1962). Intense Al absorption was found for the phenocryst cores of the Teplice rhyolite, whereas Al-absorption is less pronounced in quartz from the Schönfeld rhyodacite and from the Åland rapakivi granite. Quartz with blue CL has also relatively low total Al concentrations, as determined by EPMA (80 – 130 ppm; see Müller *et al.* 2005). On the other hand, the snowball quartz (Podlesí Dyke granite) with highest total Al concentrations (Fig. 8b) shows low Al-H-related absorption.

Quartz from the Podlesí Dyke granite (groundmass quartz), Schellerhau granite and Teplice rhyolite (phase TR1; Müller *et al.* 2005) shows a distinct absorption band at 3474 cm^{-1}, which is caused by a proton-compensated Al defect, perturbed by Li (Kats 1962).

The groundmass quartz of the Podlesí Dyke and Schellerhau granites is characterised by broad absorption bands at ~3110 and 3220 cm^{-1}. Both samples show high absorption intensities of both bands, which are assigned to the symmetrical stretching vibrations of frozen molecular water (Aines & Rossman 1984). Low absorption of frozen water exhibits the red luminescing phenocryst core of the Teplice rhyolite (phase TR2b; Müller *et al.* 2005). Blue luminescing quartz and snowball quartz do not show water-related absorption. These bands cannot be attributed to condensated ice in the cooling stage. The bands have been only recognized for secondary quartz and some red luminescing growth zones. Similar absorption bands as frozen molecular water may point at water-bearing micropores; the analysed quartz volume is free of visible fluid inclusions.

Sharp absorption bands at 3365, 3305 and 3474 cm^{-1} and broad absorption bands 3110 and 3220 cm^{-1} as recorded for the cores and the rims of zoned quartz (phenocrysts, snowball quartz) and in unzoned crystals (groundmass quartz) do not show distinct variation. We found however variations of the absorption pattern between different quartz types in the same rock, *e.g.*, between groundmass quartz and snowball quartz (Podlesí Dyke granite) and between the primary (igneous) quartz and secondary quartz.

7. Discussion

7.1. CL properties and trace elements of igneous quartz

Cathodoluminescence and trace element studies show that hydrogen-related defect structures are abundant in igneous quartz. According to Stevens Kalceff & Phillips (1995) the red CL emission around 1.96 eV is related to non-bridging oxygen hole centre (NBOHC, an oxygen dangling bond; $\equiv$Si$-$O·) with hydrogen as precursor ($\equiv$Si$-$OH). Defect structures with hydroxyl are strongly affected by the temperature and ionising radiation: protons and hydroxyl are released and concentrate as molecular water in larger defect structures and micropores (Stenina *et al.* 1984; Heggie 1992). The increase in the red emission of igneous quartz during electron bombardment is explained by radiolysis of hydroxyl groups in the quartz lattice, which results in the formation of NBOHC. The rate of the red CL increase is moderate for early-magmatic quartz phenocrysts, but very high for quartz in the granitic ground mass.
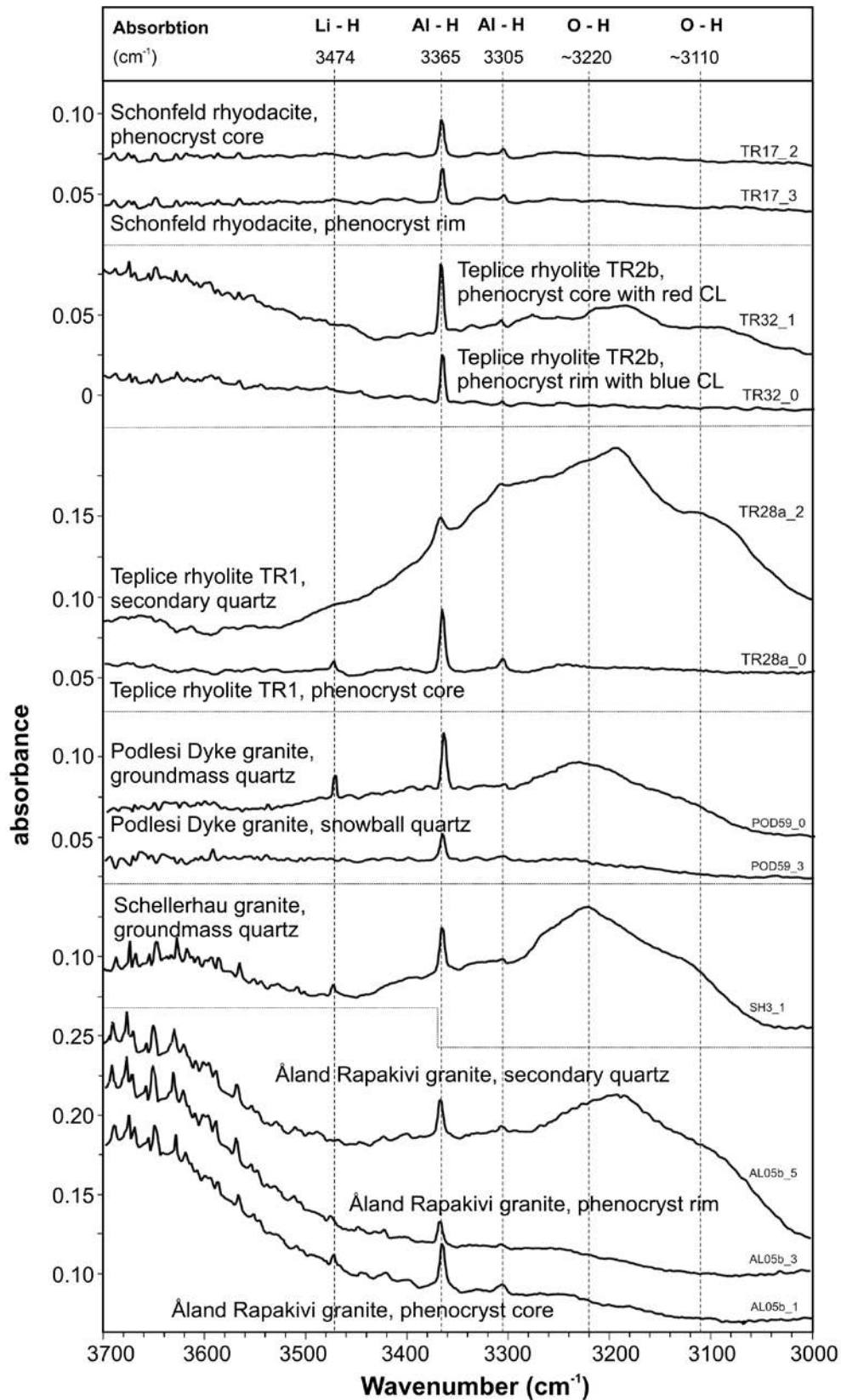
Figure 9 FTIR absorption spectra of igneous quartz. Spectra are offset for clarity.

Small, nearly non-luminescing 1-5 µm small spots have been observed in granitic groundmass quartz during electron bombardment at high beam current (*e.g.,* Fig. 6d). Stenina *et al.* (1984) described similar spots in quartz, which was intensively exposed to electron radiation. By using TEM imaging these authors identified these structures as amorphous (non-crystalline) micro-domains, which contain molecular water. The dull-luminescing spots may be explained by diffusion of protons, hydroxyl and probably also molecular water migrate ("jump") along weak donor-acceptor bonds through the quartz lattice under excitation (Heggie 1992). At defects hydroxyl and molecular water are trapped forming water-rich disordered domains. This disorder results in the local quenching of the cathodoluminescence. The elevated concentrations of molecular water in granitic groundmass quartz and secondary quartz as detected by FTIR spectroscopy confirm the existence of water-bearing micropores.

The non-luminescing micro-domains and molecular water have not been detected in early-magmatic phenocrysts with dominant blue CL. The relatively homogeneous concentration of structural hydroxyl in the quartz phenocrysts can be explained by the fact that the amount of structural hydroxyl in quartz correlates with substitutional Al. In summary, the structurally bound hydrogen and water is lowest in the early-magmatic phenocrysts and highest in the granitic groundmass. This observation verifies progressively higher water content of the melt during magma evolution. The strong increase of red-CL and the formation of water-rich disordered micro-domains in granitic groundmass quartz reflects crystallisation from a cool and water-enriched melt. Consequently, late-magmatic snowball quartz should contain highest concentrations of structural water. However, we found lowest structural water here. This unexpected result is related to very rapid quartz crystallization in F-, B-, and/or P-enriched magmas, because hydrogen diffusion within the quartz lattice requires time to operate. The low-pressure (subsurface) quartz growth would add to the effect of rapid growth, because the hydroxyl content in quartz is a positive function of pressure (e.g., Mosenfelder 2000). In this specific environment quartz incorporates only traces of hydroxyl which are below the detection limit of FTIR spectrometry.

The "flash" of blue CL commonly observed during the first seconds of electron bombardment is caused by an emission band at 3.18-3.26 eV (Alonso *et al.* 1983, Luff & Townsend 1990, Perny *et al.* 1992, Gorton *et al.* 1996) According to these authors the intensity of the emission band correlates well with the Al content and the concentration of paragenetic [AlO_4/M^+]. The band position lies outside the sensitivity range of the spectrometer used in this study. About 1600 analyses of total Al concentration in quartz do not show a clear correlation with one of the 9 emission bands, which were detected for igneous quartz between 1.4 and 3.1 eV (Müller 2000, this study). This lack of correlation may be attributed to the different atomic configurations of Al in the quartz lattice. The substitutional trivalent Al^{3+} can be compensated by coupled substitution of a pentavalent ion, *e.g.* P^{5+}, or by interstitial monovalent ions such as Li^+, H^+, Na^+ and K^+. Therefore, Al in quartz depends on the availability of the compensating ions in the crystallising melt. The different valences of Al in quartz require different uptake conditions. The larger part of the total Al in quartz is probably incorporated in sub-microscopic defect clusters (<0.2 µm) as discussed by Müller *et al.* (2003a). The higher concentration of defect clusters as detected here particularly for quartz with >500 ppm Al, explains the contradictory low Al-H infrared absorption and the high total Al in the snowball quartz from Podlesí.

The intensities of the detected blue emissions at 2.58, 2.68, and 2.79 eV also decrease during electron bombardment and contribute to the initial blue "flash". Correlations between the 2.58, 2.68 and 2.79 eV emissions and the total content of Al, Ti, K, Fe could not be found. The 2.68 and 2.79 eV emissions are due to the recombination of a so-called self-trapped exciton (Stevens Kalceff & Phillips 1995), whereas the 2.58 eV band cannot be fully explained (*e.g.,* Gritsenko & Lisitsyn 1985). The self-trapped exciton involves an irradiation-induced electron hole pair (oxygen Frenkel pair consisting of an oxygen vacancy and a peroxy

linkage) and is a consequence of strong electron-phonon interactions in the SiO_2 crystal structure (Fisher *et al.* 1990). The CL emission at 2.75-2.80 eV is more or less present in all quartz types (*e.g.,* Müller 2000, Götze *et al.* 2001). Thus the defects related to the 2.58, 2.68 and 2.79 eV emissions are not only formed during crystal growth, but also induced by ionising radiation and, therefore not indicative for igneous processes.

Müller *et al*. (2002b) showed that high Ti (>50 ppm) in quartz correlates positively with the intensity of the blue 2.96 eV CL emission. It is still under debate whether Ti is a CL activator or sensitizer (Marshall 1988, Götze 2000). The increasing Al/Ti ratio during magmatic differentiation indicates that Ti is compatible during the formation of igneous quartz, whereas Al is incompatible. Wark & Watson (2006) proved that $Ti^{4+} – Si^{4+}$ substitution is temperature-dependent. The temperature dependence of Ti in quartz explains the higher content in the early-magmatic quartz phenocrysts and the systematic lower concentrations in the younger quartz generations. The relatively stable, blue-dominated CL and the relatively high abundance of Ti in early-magmatic quartz phenocrysts in volcanic rocks and some granites reflect crystallisation from a hot and relatively water-poor melt.

Pott & McNicol (1971) and Kempe *et al*. (1999) found that concentration of bound Fe^{3+} is related to the 1.73 eV CL emission. Some rhyolitic quartz phenocryst margins and the co-genetic fine-grained groundmass quartz show stable red CL at 1.73 eV and elevated Fe concentrations. However, there is no general correlation of total Fe and the 1.73 eV emission intensity found (Müller 2000). It has been frequently observed that quartz adjacent to Fe-rich minerals (biotite, hornblende, tourmaline, etc.) becomes exponentially enriched in Fe towards the grain contact up to several thousands ppm (Penniston-Dorland 2001, Müller *et al.* 2002b, 2003b). However, the diffusing ion is preferentially Fe^{2+}, due to its smaller ion radius. Fe diffuses up to 400 µm into the quartz, but the Fe-enrichment of quartz does not necessarily result in changing CL properties. Therefore, the total Fe content in quartz cannot be used to trace magmatic processes.

Schrön *et al*. (1982) introduced the ternary Ti-Al-Ge diagram to discriminate igneous quartz of different origin ("rhyolitic", "granitic" and "pegmatitic"). They showed that Ge behaves as an incompatible element during magma differentiation and is a useful quartz fingerprint for magma evolution. Jacamon & Larsen (2009) suggest that the Ge/Ti ratio in quartz is an index of the magmatic evolution of silica-saturated melts. However, the increase of Ge in quartz with increasing differentiation is only minor until the pegmatitic-pneumatolytic stage, making Ge a useful element for identifying pegmatitic quartz (Schrön *et al.* 1988, Götze *et al.* 2004). Götze *et al*. (2005) detected a correlation of the 2.45 eV emission with the concentration of the paramagnetic $[GeO_4/Li^+]^0$ center in pegmatitic quartz.

7.2. Resorption of quartz phenocrysts

Major resorption surfaces observed in early-magmatic phenocrysts in extrusive and plutonic rocks are attributed to profound changes in temperature and magma composition. These surfaces are associated with a concentration step of Ti and commonly have wavy (Fig. 5f), dendritic (Fig. 6a), or granophyric textured overgrowth. Foreign particles adhere at the freshly resorbed surface due to its roughness and the high number of free bonds. The particles cause physical shielding disturbing the planar growth of the crystal face. The hindered growth may cause growth embayments and wavy textures after major resorption events, which can be filled later on with melt droplets and foreign crystals (Figs. 5g). Minor quartz resorption reflects small changes in the same parameters caused by local magma dynamics (convection). Possible causes of major episodes of quartz resorption were previously discussed by Müller *et al.* (2003b) and Müller *et al.* (2005) on the example of the Slavkov microgranites and the igneous rocks of the eastern Erzgebirge volcano-plutonic complex. Two possible processes for major resorption of quartz crystals have been extracted from these discussions: First,

isothermal decompression due to *semi-adiabatic magma ascent* and, second, *mixing and mingling of different magmas* by injection or recharge. Both processes can be related.
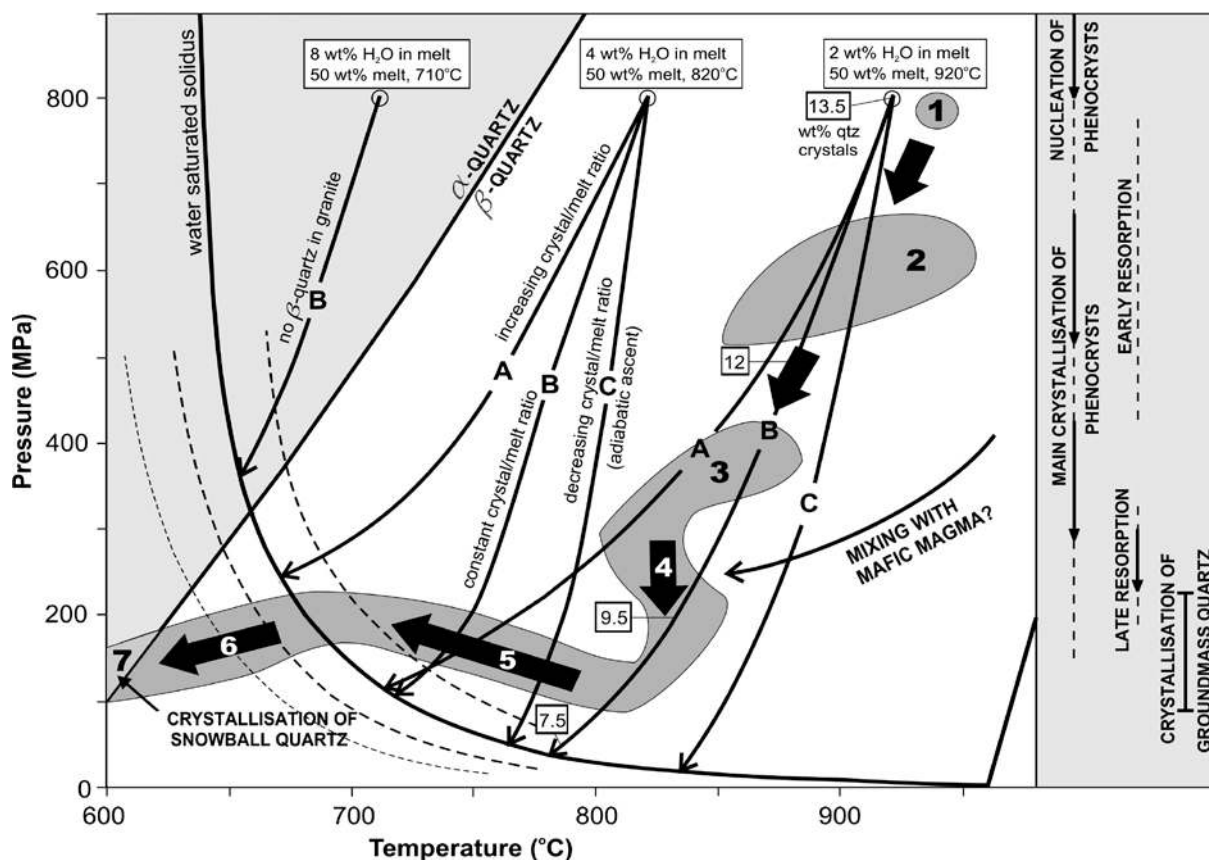

Figure 10 P-T path interpretations for quartz. The grey areas frame thermobarometric results obtained from melt inclusions in felsic igneous rocks from the Erzgebirge, Germany, by Thomas (1994). The data are compiled with experimental PT paths (A, B, and C) for haplogranitic magmas with different initial water content (Johannes & Holtz 1996). A paths = increasing crystal/melt ratio (decompression crystallisation), B paths = constant crystal melt ratio, C paths = decreasing crystal/melt ratio (decompression melting). To provide an example the change of the quartz crystal proportion in the ascending magma along the path B with the initial conditions of 920°C and 800 MPa is given according to Johannes & Holtz (1996). The quartz portion decreases but feldspar portion increases and the crystals/melt ratio remains constant. Values for the β-/α-quartz inversion are from Yoder (1950). The dashed solidus lines illustrate the variability of the solidus for different granite compositions. See text for explanation of numbers 1 to 7.

Semi-adiabatic magma ascent. Strong resorption of quartz crystals may occur during semi-adiabatic magma ascent for an energetically closed system (Johannes & Holtz 1996; Fig. 10). Decompression melting during isothermal magma ascent is mainly caused by the decrease of the minimum H_2O content of the melt leading to the increase of the ratio H_2O_{total}/H_2O_{melt} in the system (Tuttle & Bowen 1958; Carmichael *et al.* 1974; Sykes & Holloway 1987; Holtz & Johannes 1994; Johannes & Holtz 1996). Experimental data of Johannes & Holtz (1996) obtained for the haplogranite system and illustrated in Fig. 10 are used here for better understanding the processes of possible quartz resorption during magma ascent. Fig. 10 shows the experimental ascent paths of 3 haplogranitic magmas with 2, 4, and 8 wt.% H_2O in the melt according Johannes & Holtz (1996). The water-undersaturated magmas start to rise at 800 MPa with 50 wt.% melt and 50 wt.% crystals. During crystallisation along path A the crystal/melt ratio is increased (decompression crystallisation). Path B represents magma ascent at constant crystal/melt ratio. In the case of an ascending melt along path B with 2 wt.% H_2O in the melt and 920°C initial temperature, the relative proportion of quartz and

feldspar changes, but the crystals/melt ratio remains constant. Before the solidus is reached the proportion of quartz is lowered from 13.5 wt.% to 7.5 wt.% (Fig. 10). On the other hand nearly isothermal decompression (path C), corresponding to adiabatic magma ascent, is accompanied by the release of H_2O from the melt in a chemically and energetically closed system. Higher water activities result in melting of the crystals and formation of additional melt (decompression melting). In the C path example with the initial ascent conditions 800 MPa and 820°C, about 30 vol.% of quartz and feldspar crystals would dissolve between 800 and 50 MPa (Johannes & Holtz 1996). Crystal resorption is much more intense between 300 and 50 MPa than at higher pressures. The simultaneous fractionation of H_2O-free phases like quartz and feldspar may result in secondary boiling and magma ascent up to the surface. The magma evolution along path B or C is relatively short when it starts to rise at 710°C, 800 MPa, and 8 wt.% total H_2O, as the magma would crystallise completely at 12 and 8 km, respectively. The magma would become more or less immobile along the A-path and it would crystallise at 600 MPa or even higher pressures. Therefore the development of major resorption textures in quartz requires an episode of about isothermal decompression, as illustrated for paths B and C.

Table 3 Increase of quartz crystallisation temperature after major resorption episodes documented by the chemical zoning of quartz phenocrysts. Ti concentrations were determined by EPMA. a_{TiO2} - TiO_2 activity of magma according Hayden *et al.* (2005), ΔT – change of magma temperature, n – number of analyses.

name of igneous rock	magmatic province	a_{TiO2}	location of resorption surface within phenocrysts	Ti (ppm) of quartz prior to resorption	Ti (ppm) of quartz after resorption	minimum ΔT after quartz resorption (°C)
Teplice rhyolite (TR2b)	Eastern Erzgebirge, Germany	0.8	core	<22 (n=2)	58 (n=6)	+97±2
Schellerhau granite	Eastern Erzgebirge, Germany	0.8	core	<22 (n=10)	58 (n=2)	+97±2
Altenberg-Frauenstein microgranite	Eastern Erzgebirge, Germany	1	core	<33 (n=10)	59 (n=11)	+58±1
Altenberg-Frauenstein microgranite	Eastern Erzgebirge, Germany	1	marginal	59 (n=11)	120 (n=4)	+82±1
Beucha granite	NW Saxony, Germany	1	marginal (Fig. 5h)	28 (n=9)	88 (n=26)	+118±2
Hammarudda porphyry	Åland, Finland	1	marginal	154 (n=16)	211 (n=7)	+44±1

The P-T path of rhyolite and granite magmas of the Erzgebirge obtained from microthermometric studies of silicate melt inclusions by Thomas (1992, 1994) is illustrated in Figure 10, together with the generalised quartz textures and populations of quartz (Müller *et al.* 2005). The maximum pressure of 780 MPa obtained from melt inclusions represents the minimum crystallisation depth of early magmatic quartz phenocrysts of the Erzgebirge granites and rhyolites (nr. 1 in Fig. 10). It is however possible that phenocrysts originate from greater depth. For example, rhombohedric α-quartz phenocrysts in rhyolites of the Odenwald (Dossenheim and Weinheim rhyolite, Germany; Fig. 5c) and other occurrences (Bozen rhyolite, Italy) indicate much deeper quartz crystallization (Flick 1987). Flick (1987)

suggested a minimum crystallisation pressure of the α-quartz phenocrysts at 1250 to 1400 MPa assuming a magma temperature between 900 and 950°C. The P-T-path of the Erzgebirge granites and rhyolites (Thomas 1992, 1994) follows roughly the experimental determined paths A and B for haplogranitic melts with 1.5 to 2.5 wt.% H_2O in melt (Johannes & Holtz 1996).

The path of the Erzgebirge magmas is not well documented between 800 and 400 MPa so that ascent parameters may correspond to the path A, B or even C. A number of phenocryst populations in the Eastern Erzgebirge contain rounded crystal cores, which indicate resorption during the early stage of crystallisation (Fig. 5d; Müller *et al.* 2005). This early resorption episode can be attributed to rapid magma ascent or magma mixing. Temporary magma storage occurred probably between 17-24 km (nr. 2) and in the ductile-brittle transition zone between 13-10 km depth (nr. 3; Müller *et al.* 2000, 2005). These stages are documented by significant amounts of quartz growth. Decompression crystallisation (path A) must have occurred between 400 and 300 MPa (between nr. 2 and 3) resulting in higher water contents in the melt. Melt inclusion data indicate adiabatic magma ascent (path C) between 10-4.5 km depth (nr. 4) that possibly caused quartz phenocryst resorption. An increase of magma temperature could have been caused by mixing with mafic magma. Most of the Erzgebirge magmas were emplaced at shallow depth of 5-2.6 km. Here, the solidifying magmas became supersaturated in volatiles and the pressures only slightly increased along the solidus (nr. 5). Melt inclusion data on the left side of the haplogranite solidus (nr. 6) reflect chemistries of highly fractionated magmas enriched in fluorine and other volatiles causing a shift of the solidus. Finally, igneous α-quartz crystallised in topaz-bearing albite granites (nr. 7).

Magma mixing: A number of late-Hercynian rhyolites and granites contain phenocrysts with major resorption surfaces, which were affected by magma mixing and mingling (Müller *et al.* 2005). Rock-forming minerals in these rocks show textures, which indicate magma mixing, like plagioclase-mantled K-feldspar, sieve-textured plagioclase and mafic micro enclaves (Müller *et al.* 2005). The pre-resorption growth zones in these quartz phenocrysts are in some cases smudged and blurred, whereas the boundaries of post-resorption growth zones are sharp. The smudging of pre-resorption growth zones is explained by the redistribution and healing of defect centres in quartz (Müller *et al.* 2005). Smudging of growth zoning in quartz is, however, a rare phenomenon among the late-Hercynian igneous rocks.

The Ti-in-quartz geothermometer of Wark & Watson (2006) provides a tool to determine the quartz crystallisation temperature prior to and after a major phenocryst resorption episode. Table 3 shows calculations of the minimum temperature change after a major resorption episode. The Ti activity a_{TiO2} in the magma was determined according Hayden *et al.* (2005). Rutile and titanomagnetite are common accessories in the Altenberg-Frauenstein microgranite, Beucha granite, and Hammerrudda porphyry indicating Ti saturation of the magma. Rutile is rare in the Teplice rhyolite and Schellerhau granite which implies slight Ti undersaturation which is confirmed by the calculation method by Hayden *et al.* (2005). The magma temperature increase in all cases is significant. If the resorption is caused by semi-adiabatic magma ascent the magma moves into a higher and cooler crustal level and the Ti in quartz would not increase after resorption. The findings support the hypothesis that major resorption of quartz phenocrysts is caused by mixing and mingling with a more mafic magma.

Thus, a number of strong resorption episodes can be related to magma mixing and mingling, particularly, to those observed in igneous rocks of the eastern Erzgebirge volcano-plutonic complex (Müller *et al.* 2005). However, most of the other igneous rocks discussed here show no chemical or textural evidence for magma mixing. These rocks were possibly affected by multiple magma recharge (stepwise magma ascent) resulting in acid-acid magma mixing and mingling. Semi-adiabatic magma ascent theoretically causes major resorption of

quartz crystals. At present there is no strong evidence for this theory. However, the injection of a hotter (more mafic) magma at the deeper levels of a magma reservoir may lead to higher gas pressures and trigger magma ascent (*e.g.,* Blake *et al.* 1992, Smith *et al.* 2004). It is suggested that magma mixing and adiabatic magma ascent go normally hand in hand during the magma evolution, as was demonstrated in the example of the Erzgebirge Granites.

8. Summary

CL spectra of igneous quartz in late-Hercynian volcanic and plutonic rocks in central and western Europe commonly comprise 9 emission bands between 1.4 and 3.1 eV. The decay of blue luminescing centres and generation of red luminescing centres during electron bombardment have been quantified by applying the kinetic law. Granitic groundmass quartz has more unstable CL, in particular the red 1.85 and 1.96 eV emissions, than the CL of early-magmatic quartz phenocrysts. The increase of the 1.85 and 1.96 eV emissions during electron radiation is explained by the radiolysis of OH- and H_2O-defects in quartz. The formation of water-rich disordered micro-domains and the strong increase of red-CL in granitic groundmass quartz reflects crystallisation from a water-rich melt in the emplacement level when the melt became rich in water. CL contrasts among growth zones in zoned quartz phenocrysts are essentially related to the distribution of trace elements. Blue luminescing growth zones have high Ti (>50 ppm). High intensity of the relatively stable blue emission at 2.96 eV correlates with high Ti in quartz. As differentiation proceeds the Ti concentration in quartz decreases, whereas Al in quartz increases. Thus, Ti behaves compatibly during the evolution of igneous quartz whereas Al behaves more incompatibly. The more stable, blue-dominated CL and the relative high abundance of Ti in quartz phenocrysts in rhyolites and a number of granites reflect higher crystallisation temperatures and a lower crust origin.

CL reveals complex growth patterns of early-magmatic quartz phenocrysts in late-Hercynian volcanic and plutonic rocks. Fine-scale (<10 µm) oscillatory zoning, large-scale step zoning with strong CL contrasts, skeletal growth, resorption surfaces, and growth embayments are distinguished. A few of late-Hercynian granites contain quartz phenocryst populations similar to phenocrysts in associated rhyolites, indicating that the rhyolite is the extrusive equivalent of the underlying granite. Examples are known from the Eastern Erzgebirge volcano-plutonic complex, *e.g.* the Schellerhau granites and Teplice rhyolites (Müller *et al.* 2005). This phenomenon is presumably much more common but rhyolites associated with Hercynian granites are either eroded or have not been developed. Phenocrysts in granites are embedded in unzoned anhedral groundmass quartz that makes their identification difficult. A number of major resorption episodes can be related to mixing of magmas with different physicochemical properties. There is no strong evidence that the observed major resorption surfaces are caused by semi-adiabatic magma ascent. However, both causes can be related, because the injection or recharge of mafic and hotter magmas into the bottom of felsic magma reservoirs may trigger the rise of felsic magma portions.

There are still, however, a number of open questions regarding the petrogenetic significance of the CL properties and the trace element signature of igneous quartz. In particular, the crystallisation parameters, which control the incorporation of Al into the quartz lattice have to be evaluated by experimental work.

10. References

Aines, R.D. & Rossman, G.R. 1984. Water in minerals? A peak in the infrared. *Journal of Geophysical Research* **89/B6**, 4059-4071.

Allègre, C.J., Provost, A. & Jaupart, C. 1981. Oscillatory zoning: A pathological case of crystal growth. *Nature* **294,** 223-228.

Alonso, P.J., Halliburton, L.E., Kohnke, E.E. & Bossoli, R.B. 1983. X-ray induced luminescence in crystalline SiO_2. *Journal of Applied Physics* **54**, 5369-5375.

Armstrong, J.T. 1995. CITZAF: A package of correction programs for the quantitative electron microbeam X-ray analysis of thick polished materials, thin films, and particles. *Microbeam Analysis* **4,** 177-200.

Bahadur, H. 1994. Sweeping and irradiation effects on hydroxyl defects in crystalline natural quartz. *IEEE Transactions on Ultrasonics, Ferroelectrics and Frequency Control* **41/6**, 820-833.

Bambauer, H.U., Brunner, G.O. & Laves, F. 1963. Merkmale des OH-Spektrums alpiner Quarze (3μ-Gebiet). *Schweizerische Mineralogische und Petrographische Mitteilungen* **43**, 259-268.

Behr, H.J. 1989. Die geologische Aktivität von Krustenfluiden. *In Gesteinsfluide - Ihre Herkunft und Bedeutung für geologische Prozesse.* Hannover: Niedersächsische Akademie der Geowissenschaften Veröffentlichungen. Vol. 1, 7-42.

Behr, H.-J. & Frentzel-Beyme, K. 1989. Permeability and paleoporosity in crystalline bedrocks of the Central European basement-studies of cathodoluminescence. *In* Boden, A.& Eriksson, K.G. (eds.) *Exploration of the deep continental crust. Deep drilling in crystalline bedrock.* Vol. 2, 477-497. Berlin Heidelberg New York: Springer.

Beus, A.A., Severov, E.A., Sitnin, A.A. & Subbotin, K.D. 1962. Albitized and greisenized granites (apogranites). Moscow: Nauka (in Russian).

Blake, S., Wilson, C.J.N., Smith, I.E.M. & Walker, G.P.L. 1992. Petrology and dynamics of the Waimihia mixed magma eruption, Taupo volcano, New Zealand. *Journal of the Geological Society of London* **149**, 193-207.

Blankenburg, H.-J., Götze, J. & Schulz, J. 1994. *Quarzrohstoffe*. Deutscher Verlag für Grundstoffindustrie, Leipzig-Stuttgart, Germany.

Botis, S., Nokhrin, S.M., Pan, Y., Xu, Y. & Bonli, T. 2005. Natural radiation-induced damage in quartz. I. Correlations between cathodoluminescence colors and paramagnetic defects. *Canadian Mineralogist* **43,** 1565-1580.

Breiter, K., Müller, A., Leichmann, J. & Gabašova, A. 2005. Textural and chemical evolution of a fractionated granitic system: the Podlesí stock, Czech Republic. *Lithos* **80**, 323-345.

Carmichael, I.S.E., Turner, F.J. & Verhoogen, J. 1974. Igneous petrology. New York, McGraw-Hill.

Charlier, B.L.A., Wilson, C.J.N., Lowenstern, J.B., Blake, S., van Calsteren, P.W. & Davidson, J.P. 2005. Magma generation at a large, hyperactive silicic volcano (Taupo, New Zealand) revealed by U-Th and U-Pb systematic in zircons. *Journal of Petrology* **46,** 3-32.

Davidson, J., Tepley III, F., Palacz, Z. & Meffan-Main, S. 2001. Magma recharge, contamination and residence times revealed by in situ laser ablation analysis of feldspar in volcanic rocks. *Earth and Planetary Science Letters* **184**, 427-442.

Davidson, J., Morgan D.J., Charlier, B.L.A., Harlou, R. & Hora, J.M. 2007. Microsampling and isotopic analysis of igneous rocks: Implications for the study of magmatic systems. *Annual Reviews of Earth and Planetary Sciences* **35**, 273-311.

D'Lemos, R.S., Kearsley, A.T., Pembroke, J.W., Watt, G.R. & Wright, P. 1997. Complex quartz growth histories in granite revealed by scanning cathodoluminescence techniques. *Geological Magazine* **134**, 459-552.

Fenn, P.M. 1977. The nucleation and growth of alkali feldspars from hydrous melts. *Canadian Mineralogist* **15,** 135-161.

Fenn, P.M. 1986. On the origin of graphic granite. *American Mineralogist* **71,** 325-330.

Fisher A. J., Hayes W. & Stoneham A. M. 1990. Structure of the self-trapped exciton in quartz. *Physical Reviews Letters* **64**, 2667 – 2670.

Flick, H. 1987. Geotektonische Verknüpfung von Plutonismus und Vulkanismus im südwestdeutschen Variscicum. *Geologische Rundschau* **76**, 699-707.

Fowler, A.D. 1990. Self-organized mineral textures of igneous rocks: the fractal approach. *Earth Sciences Reviews* **29,** 47-55.

Gorton, N.T., Walker, G. & Burley, S.D. 1996. Experimental analysis of the composite blue CL emission in quartz. *Journal of Luminescence* **72-74**, 669-671.

Götze, J. 2000. Cathodoluminescence microscopy and spectroscopy in applied mineralogy. *Freiberger Forschungshefte* **C 485**, 1-128.

Götze, J. & Plötze, M. 1997. Investigation of trace element distribution in detrital quartz by electron paramagnetic resonance (EPR). *European Journal of Mineralogy* **9**, 529-537.

Götze, J., Plötze, M. & Habermann, D. 2001. Origin, spectral characteristics and practical applications of the cathodoluminescence (CL) of quartz – a review. *Mineralogy and Petrology* **71**, 225-250.

Götze, J., Plötze, M. Graupner, T., Hallbauer, D.K., Bray, C.J. 2004. Trace element incorporation into quartz: A combined study by ICP-MS, electron spin resonance, cathodoluminescence, capillary ion analysis, and gas chromatography. *Geochimica et Cosmochimica Acta* **68**, 3741-3759.

Götze, J., Plötze, M. & Trautmann, T. 2005. Structure and luminescence characteristics of quartz from pegmatites. *American Minerlogist* **90,** 13-21.

Gritsenko, B.P. & Lisitsyn, V.M. 1985. Intrinsic short-lived defects in quartz. *Soviet Physics - Solid State* **27**, 1330-1331.

Gurbanov, A.G., Chernukha, D.G., Koshchug, D.G., Kurasova, S.P. & Fedyushchenko, S.V. 1999. EPR spectroscopy and geochemistry of rock-forming quartz as an indicator of the superimposed processes in rocks of igneous associations of various ages in the Greater Caucasus. *Geochemistry International* **37,** 519-604.

Hayden, L.A., Watson, E.B. & Wark, D.A. 2005. Rutile saturation and TiO_2 diffusion in hydrous siliceous melts. *EOS Transactions, American Geophysical Union* **86**, Fall meeting supplement, MR13A-0076.

Heggie, M.I. 1992. A molecular water pump in quartz dislocations. *Nature* **355,** 337-339.

Holtz, F. & Johannes, W. 1994. Maximum and minimum water contents of granitic melts: implications for chemical and physical properties of ascending magmas. *Lithos* **32,** 149-159.

Itoh, C., Suzuki, T. & Itoh, N. 1990. Luminescence and defect formation in undensified and densified amorphous SiO_2. *Physical Reviews B* **41/6,** 3794-3799.

Jacamon, F. & Larsen, R.B. 2009. Trace element evolution of quartz in the charnockitic Kleivan granite, SW Norway: The Ge/Ti ration of quartz as an index of igneous differentiation. *Lithos* **107**, 281-291.

Jani, M., Halliburton, L.E. & Kohnke, E.E. 1983. Point defects in crystalline SiO_2: thermally stimulated luminescence above room temperature. *Journal of Applied Physics* **54**, 6321-6328.

Johannes, W. & Holtz, F. 1996. *Petrogenesis and experimental petrology of granitic rocks.* Springer, Berlin, Heidelberg, New York.

Kats, A. 1962. Hydrogen in alpha-quartz. *Philips Research Reports* **17**, 133-279.

Kempe, U., Götze, J., Dandar, S. & Habermann, D. 1999. Magmatic and metasomatic processes during formation of the Nb-Zr-REE deposits from Khaldzan Buregte (Mongolian Altai): Indications from a combined CL-SEM study. *Mineralogical Magazine* **63,** 165-177.

Kirkpatrick, R.J. 1981. *Kinetics of crystallization of igneous rocks.* Reviews in Mineralogy vol. 8**,** 321-398. Washington D.C.: Mineralogical Society of America.

Kovalenko, V.I. 1977. Petrology and geochemistry of rare-metal granitoids. Novosibirsk: Nauka (in Russian).

Kronenberg, A.K., Kirby, S.H., Aines, R.D. & Rossmann, G.R. 1986. Solubility and diffusional uptake of hydrogen in quartz at high water pressures: implications for hydrolytic weakening in the laboratory and within the earth. *Tectonophysics* **172**, 255-271.

Laemmlein, G. 1930. Korrosion und Regeneration der Porphyr-Quarze. *Zeitschrift für Kristallographie* **75**, 109-127.

Larsen, R.B., Polvé, M. & Juve, G. 2000. Granite pegmatite from Evje-Iveland: trace element chemistry and implications for the formation of high-purity quartz. *Norges geologiske undersøkelse Bulletin* **436,** 57-65.

Larsen, R.B., Henderson, I., Ihlen, P.M. & Jacamon, F. 2004. Distribution and petrogenetic behaviour of trace elements in granitic quartz from South Norway. *Contributions to Mineralogy and Petrology* **147**, 615-628.

Luff, B.J. & Townsend, P.D. 1990. Cathodoluminescence of synthetic quartz. *Journal of Physics: Condensed Matter* **2,** 8089-8097.

Lyakhovich, V.V. 1972. *Trace elements in rock-forming minerals of granitoids.* Moscow: Izd. Nedra, 200 pp. (in Russian)

Mashima, H. 2004. Time scale of magma mixing between basalt and dacite estimated for the Saga–Futagoyama volcanic rocks in northwest Kyushu, southwest Japan. *Journal of Volcanology and Geothermal Research* **131**, 333-349.

Marshall, D.J. 1988. *Cathodoluminescence of geological materials.* Winchester/Mass.: Allen & Unwin Inc.

Mosenfelder, J.L. 2000. Pressure dependence of hydroxyl solubility in coesite. *Physics and Chemistry of Minerals* **27**, 610-617.

Müller, A. 2000. *Cathodoluminescence and characterisation of defect structures in quartz with applications to the study of granitic rocks.* Ph.D. Thesis, University Göttingen, Germany.

Müller, A. & Seltmann, R. 1999. The genetic significance of snowball quartz in high fractionated tin granites of the Krušne Hory/Erzgebirge. *In* Stanley, C.J. et al. (eds.) *Mineral deposits: processes to processing*, Vol. 1, 409-412. Rotterdam: Balkema, The Netherlands.

Müller, A., Seltmann, R. & Behr, H.J. 2000. Application of cathodoluminescence to magmatic quartz in a tin granite – case study from the Schellerhau Granite Complex, Eastern Erzgebirge, Germany. *Mineralium Deposita* **35**, 169-189.

Müller, A., Kronz, A. & Breiter, K. 2002a. Trace elements and growth pattern in quartz: a fingerprint of the evolution of the subvolcanic Podlesí Granite System (Krušné Hory, Czech Republic). *Bulletin of Czech Geological Survey* **77**, 135-145.

Müller, A., Lennox, P. & Trzebski, R. 2002b. Cathodoluminescence and micro-structural evidence for crystallisation and deformation processes of granites in the Eastern Lachlan Fold Belt (SE Australia). *Contributions to Mineralogy and Petrology* **143**, 510-524.

Müller, A., Wiedenbeck, M., Van den Kerkhof, A.M., Kronz, A. & Simon, K. 2003a. Trace elements in quartz – a combined electron microprobe, secondary ion mass spectrometry, laser-ablation ICP-MS, and cathodoluminescence study. *European Journal of Mineralogy* **15**, 747-763.

Müller, A., René, M., Behr, H.-J. & Kronz, A. 2003b. Trace elements and cathodoluminescence of igneous quartz in topaz granites from the Hub Stock (Slavkovský Les Mts., Czech Republic). *Mineralogy and Petrology* **79**, 167-191.

Müller, A., Breiter, K., Seltmann, R. & Pécskay, Z. 2005. Quartz and feldspar zoning in the Eastern Erzgebirge pluton (Germany, Czech Republic): evidence of multiple magma mixing. *Lithos* **80**, 201-227.

Müller, A., Seltmann, R., Halls, C., Jeffries, T., Dulski, P., Spratt, J. & Kronz, A. 2006a. The Land's End granite, Cornwall: the evolution of a composite and mineralised pluton. *Ore Geology Reviews* **28**, 329-367.

Müller, A., Thomas, R., Wiedenbeck, M., Seltmann, R. & Breiter, K. 2006b. Water content of granitic melts from Cornwall and Erzgebirge: A Raman spectroscopy study of melt inclusions. *European Journal of Mineralogy* **18**, 429-440.

Müller, A., Ihlen, P.M. & Kronz A. 2008. Quartz chemistry in polygeneration Sveconorwegian pegmatites, Froland, Norway. *European Journal of Mineralogy*, in press

Neuser, R. D., Bruhn, F., Götze, J., Habermann, D. & Richter, D. K. 1995. Kathodolumineszenz: Methodik und Anwendung. *Zentralblatt für Geologie und Paläontologie Teil 1* **1/2**, 287-306.

Owen, M.R. 1988. Radiation-damage halos in quartz. *Geology* **16,** 529-532.

Pichavant, M. 1981. An experimental study of the effect of boron on water-saturated haplogranite at 1 kbar pressure: geological applications. *Contributions to Mineralogy and Petrology* **76**, 430– 439.

Penniston-Dorland, S.C. 2001. Illumination of vein quartz textures in a porphyry copper ore deposits using scanned cathodoluminescence: Grasberg Igneous Complex, Irian Jaya, Indonesia. *American Mineralogist* **86,** 652-666.

Pearce, T.H. & Kolisnik, A.M. 1990. Observations of plagioclase zoning using interference imaging. *Earth Science Reviews* **29,** 9-26.

Peppard, B.T., Steele, I.M., Davis, A.M., Wallace, P.J. & Anderson, A.T. 2001. Zoned quartz phenocrysts from the rhyolitic Bishop Tuff. *American Mineralogist* **86**, 1034-1052.

Perny, B., Eberhardt, P., Ramseyer, K., Mullis, J. & Pankrath, R. 1992. Microdistribution of aluminium, lithium and sodium in a quartz: possible causes and correlation with shored lived cathodoluminescence. *American Mineralogist* **77**, 534-544.

Picouet, P.A. 1999. Cathodoluminecence spectroscopy and the orientation of a hydrothermal quartz crystal. *Schweizerische Mineralogische und Petrographische Mitteilungen* **79**, 455-460.

Pott, G.T. & McNicol, B.D. 1971. Spectroscopy study of the coordination and valence of Fe and Mn ions in and on the surface of aluminas and silicas. *Discussions of the Faraday Society* **52**, 121-131.

Poutiainen, M. & Scherbakova, T.F. 1998. Fluid and melt inclusion evidence for the origin of idiomorphic quartz crystals in topaz-bearing granite from the Salmi batholith, Karelia, Russia. *Lithos* **44**, 141-151.

Rajpoot, G.S. 1991. *Controversies in geotectonics of Hercynian Europe.* Prague: Czech Geological Survey.

Ramseyer, K., Baumann, J., Matter, A. & Mullis, J. 1988. Cathodoluminescence colours of α-quartz. *Mineralogical Magazine* **52**, 669-677.

Remond, G., Cesbron, F., Chapoulie, R., Ohnenstetter, D., Rouques-Carmes, C. & Schvoerer, M. 1992. Cathodoluminescence applied to the microcharacterization of mineral

materials: a present status in experimentation and interpretation. *Scanning Microscopy* **6/1**, 23-69.

Rink, W.J., Rendell, H., Marseglia, E.A., Luff, B.J. & Townsend, P.D. 1993. Thermoluminescence Spectra of igneous quartz and hydrothermal quartz. *Physics and Chemistry of Minerals* **20**, 353-361.

Rovetta, M.R., Blacic, J.D., Hervig, R.L. & Holloway, J.R. 1989. An experimental study of hydroxyl in quartz using infrared spectroscopy and ion microprobe techniques. *Journal of Geophysical Research* **94**, 5840-5850.

Ruffini, R., Borghi, A., Cossio, R., Olmi, F. & Vaggelli, G. 2002. Volcanic quartz growth zoning identified by cathodoluminescence and EPMA studies. *Mikrochemica Acta* **139,** 151-158.

Rusk, B. & Reed, M. 2002. Scanning electron microscope-cathodoluminescence analysis of quartz reveals complex growth histories in veins from the Butte porphyry copper deposit, Montana. *Geology* **30,** 727-730.

Schneider, J. 1993. Das lumineszenzaktive Strukturinventar von Quarzphänokristen in rhyolithen. *Göttinger Arbeiten zur Geologie und Paläontologie* **60,** 1-81.

Schrön, W., Schmädicke, E., Thomas, R. & Schmidt, W. 1988. Geochemische Untersuchungen an Pegmatitquarzen. *Zeitschrift für Geologische Wissenschaften* **16,** 229-244.

Sigel, G.H. Jr. & Marrone, M.J. 1981. Photoluminescence in as-drawn and irradiated silica optical fibres: An assessment of the role of nonbridging oxygen defect centres. *Journal of Non Crystalline Solids* **45,** 235-247.

Smith, V.C., Shane, P. & Nairn, I.A. 2004. Reactivation of a rhyolitic magma body by new rhyolitic intrusion before the 15.8 ka Rotora eruptive episode: implications for magma storage in the Okataina Volcanic Centre, New Zealand. *Journal of the Geological Society of London* **161**, 757-772.

Sonyushkin, V.E., Sukhorukov, Y.T. & Scherbakova, T.F. 1991. P-T environment of crystallization of quartz in granites of the Salmi batholith, Russian Karelia. *In* Haapala, I. & Rämö, O.T. (eds.) *Symposium on Rapakivi Granites and Related Rocks*. Geological Survey of Finland Guide, vol. 34, 47.

Sprunt, E.S. 1981. Causes of quartz cathodoluminescence colors. *Scanning Electron Microscopy* **1981**, 525-535.

Sprunt, E.S. & Nur, A. 1979. Microcracking and healing in granites: New evidence from cathodoluminescence. *Science* **205**, 495-497.

Stenina, N.G., Bazarov, L.S., Shcherbakova, M.Y. & Mashkovtsev R.I. 1984. Structural state and diffusion of impurities in natural quartz of different genesis. *Physics and Chemistry of Minerals* **10**, 180-186.

Stevens Kalceff, M.A. & Phillips, M.R. 1995. Cathodoluminescence microcharacterization of the defect structure of quartz. *Physical Reviews B* **52**, 3122-3134.

Stevens Kalceff, M.A., Phillips, M.R., Moon, A.R. & Kalceff, W. 2000. Cathodoluminescence microcharacterization of silicon dioxide polymorphs. *In* Pagel, M., Barbin V., Blanc P. & Ohnenstetter D. (eds.) *Cathodoluminescence in Geosciences.* Berlin: Springer.

Suttner, L. & Leininger, R.K. 1972. Comparison of the trace element content of plutonic, volcanic and metamorphic quartz from Southwestern Montana. *Geological Society of America Bulletin* **83,** 1855-1862.

Swanson, S.E. 1977. Relation of nucleation and crystal-growth to the development of granitic textures. *American Mineralogist* **62,** 966-978.

Sykes, M.L. & Holloway, J.R. 1987. Evolution of granitic magmas during ascent: a phase equilibrium model. *In* Mysen, B.O. (ed.) *Magmatic processes: Physicochemical Principles*. Geochemical Society, Special Publication vol. 1, 447-461.

Thomas, R. 1992. Results of investigations on melt inclusions in various magmatic rocks from the northern border of the Bohemian Massif. *In* Kukal, Z. (ed.) *Proceedings of the 1st International Conference about the Bohemian Massif.* Prague: Czech Geological Survey, Prague.

Thomas, R. 1994. Fluid evolution in relation to the emplacement of the Hercynian granites in the Erzgebirge region: a review of the melt and fluid inclusion evidence. *In* Seltmann, R., Möller, P., Kämpf, H. (eds.) *Metallogeny of Collisional Orogens.* Prague: Czech Geological Survey.

Tuttle, O.F. & Bowen, N.L. 1958. Origin of granite in the light of experimental studies in the system $NaAlSi_3O_8$-$KalSi_3O_8$-SiO_2-H_2O. *Geological Society of America Memoir* **74**, 1-153.

Valley, J.W. & Graham, C.M. 1996. Ion microprobe analysis of oxygen isotope ratios in quartz from Skye granite: healed micro-cracks, fluid flow, and hydrothermal exchange. *Contributions to Mineralogy and Petrology* **124**, 225-234.

Van den Kerkhof, A.M. & Grantham, G.H. 1999. Metamorphe charnockite in contact aureoles around intrusive enderbite from Natal, South Afrika. *Contributions to Mineralogy and Petrology* **137**, 115-132.

Van den Kerkhof, A.M. & Hein, U. 2001. Fluid inclusion petrography. *Lithos* **55**, 27-47.

Van den Kerkhof, A.M. & Müller, A. 1999. Fluid inclusion re-equilibration and trace element redistribution in quartz: observations by cathodoluminescence microscopy. ECROFI XV 1999 Abstracts and Program, Potsdam, *Terra Nostra* **99/6**, 161-162.

Van den Kerkhof, A.M., Kronz, A. & Simon, K. 2001. Trace element redistribution in metamorphic quartz and fluid inclusion modification: observations by cathodoluminescence. XVI ECROFI, Porto 2001, *Departomento Geologica Memória* **7**, 447-450.

Van den Kerkhof, A.M., Kronz, A., Simon, K. & Scherer, T. 2004. Fluid-controlled quartz recovery in granulite as revealed by cathodoluminescence and trace element analysis (Bamble sector, Norway). *Contributions to Mineralogy and Petrology* **146**, 637-652.

Vollbrecht, A., Olesen, N.O., Schmidt, N.H. & Weber, K. 1994. Crystallographic microcrack orientation in quartz from a granite – a combined ECP/U stage study. *In* Bunge, H.J., Siegesmund, S., Skrotzki, W. & Weber, K. (eds.) *Textures of geological materials.* Oberursel: DGM Informationsgesellschaft Verlag.

Vollbrecht, A., Rust, S. & Weber, K. 1991. Development of microcracks in granites during cooling and uplift: examples from the Hercynian basement in NE Bavaria, Germany. *Journal of Structural Geology* **13**, 787-799.

Wark, D.A. & Watson, E.B. 2006. TitaniQ: a titanium-in-quartz geothermometer. *Contributions to Mineralogy and Petrology* **152**, 743-754.

Wark, D.A., Hildreth, W., Spear, F.S., Cherniak D.J. & Watson E.B. 2007. Pre-eruption recharge of the Bishop magma system. *Geology* **35**, 235-238.

Watt, G.R., Wright, P., Galloway, S. & McLean, C. 1997. Cathodoluminescence and trace element zoning in quartz phenocrysts and xenocrysts. *Geochimica et Cosmochimica Acta* **61**, 4337-4348.

Wiebe, R.A., Wark, D.A. & Hawkins, D.P. 2007. Insights from quartz cathodoluminescence zoning into crystallization of the Vinalhaven granite, coastal Maine. *Contributions to Mineralogy and Petrology* **154**, 439-453.

Yang, X.H., Townsend, P.D. & Holgate, S.A. 1994. Cathodoluminescence and depth profiles of tin in float glass. *Journal of Physics D* **27**, 1757-1762.

Yoder, H.R. 1950. High-low quartz inversion up to 10,000 bars. *Transactions, American Geophysical Union* **31**, 827-835.